FIRST PRINCIPLES STUDY OF STRUCTURAL, ELECTRONIC AND MECHANICAL PROPERTIES OF LANTHANUM FLUORIDE AND LANTHANUM DOPED BARIUM FLUORIDE

WABULULU ELICAH NAFULA
(Msc)
I84/33524/2014

A THESIS SUBMITTED IN PARTIAL FULFILLMENT OF THE REQUIREMENTS FOR THE AWARD OF DEGREE OF DOCTOR OF PHILOSOPHY (PHYSICS) IN THE SCHOOL OF PURE AND APPLIED SCIENCES OF KENYATTA UNIVERSITY

NOVEMBER, 2020

DECLARATION

This thesis is my original work and has not been presented for a degree or other awards in any other university.

Signature: ..... Date: .....

Elicah N. Wabululu I84/33524/2014
Department of Physics
Kenyatta University

SUPERVISORS

The work presented in this thesis was carried out by the student with our approval as University supervisors.

Signature…… Date……

Dr. Philip W.O. Nyawere
Department of Physical and Biological Sciences
Kabarak University

Signature…… Date……

Dr. Daniel B. Bem
Department of Physics
Kenyatta University

DEDICATION

To team Elicah USA who have sacrificed many things in order for me to achieve my higher education.

To my husband Vincent Masifwa Wekesa, my daughters Talitha Nekesa and Talia Mutiembu for their love, patience and emotional support.

ACKNOWLEDGEMENTS

I acknowledge the Almighty God for His providence during the period of this study. My supervisors, Dr. P.W.O Nyawere, Kabarak University and Dr. Daniel B. Bem, Kenyatta University for giving me guidance, intellectual support, and encouragement through the course of my thesis. To the Physics department of Kenyatta University, thank you for your time during the weekly seminars that were of great contribution to this work. All postgraduate students whose discussions and constant encouragements made this work successful.

My gratitude to the Computational Methods and Materials Science (CMMS) SIG-KENET group led by Prof. George Amolo, Dr. Moses Thiga, Dr. George Manyali and Dr. Kipkorir for the various meetings to discuss DFT methods.

The Computational and Theoretical Physics (MMUST) members; James Sifuna, Alima Mukasia, Gloria Murila, Manasse Kituyi, Samuel Opiyo, John Maera and Oketch Vincent gratitude for the constant encouragement and nurture towards DFT.

The 1st Advanced School on Applications of First-Principles and Molecular Simulations in Physical Sciences (Nigeria, 2018) was very resourceful on computational theory. I appreciate the Center for High Performance Computing (CHPC), Cape Town (South Africa) for the provision of High Performance Computing resources useful in all calculations in this thesis.

TABLE OF CONTENTS

LIST OF TABLES

LIST OF FIGURES

SYMBOLS AND ABBREVIATIONS

Ψ	Many body wave function
E	Hamiltonian total energy
M_1	Nuclei masses
Z_1	Nuclei charges
$\hbar$	Reduced Plank's constant
∇^2	Second derivative of gradient
BZ	Brillouin zone
DFT	Density Functional Theory
DOS	Density of state
e	Electronic charge
m	Electron mass
$\vec{R}_1$	Nuclei positions
H	Total Hamiltonian
H_e	Electron Hamiltonian
τ_i	Election position
φ_e	Electron wave-function
φ_{nucl}	Nuclei wave-function
$n_{\vec{r}}$	Charge density
$v_{\vec{r}}$	Ground state potential
E_{xc}	Exchange correlation energy
$F[n(r)]$	Universal functional
T	Kinetic energy
$\in_k$	Lagrange multiplier

$\in_{xc}^{hom}$	Homogeneous exchange correlation
T_c	Phase transition temperature
σ	Ionic conductivity
ΔE	Defect formation energy
k_B	Boltzmann constant
C''	Shear modulus
E_i	Energy of crystal with interstitial
H_B	Born-oppenheimer Hamiltonian
∇	Partial differential
B	Bulk modulus
DFT	Density functional theory
KS	Kohn-Sham
HK	Hohenberg-Kohn
PAW	Projected augmented wave
USPP	Ultrasoft pseudo-potentials
LAPW	Linearized augmented plane wave
LDA	Local density approximations
GGA	Generalized gradient approximation
eV	Electron-volts
F	Fluorine
GGA	Generalized gradient Approximation
Gpa	Giga Pressure
GRACE	Graphing Advanced Computing and Exploration of data
HF	Hatree Fock
IR	Infrared

La	Lanthanum
LED	Light-emitting diode
PBE	Perdew Burke Ernzerhof
scf	Self consistent field
UV	Ultra Violet
VASP	Vienna Ab initio Simulation Package
XcrysDen	X-window Crystalline Structure and density
Xe	Xenon
Z	Atomic number

ABSTRACT

Lanthanum Fluoride (LaF_3) has several applications for instance, in electrodes manufacture, fluorescent lamps and fiber optic devices due to its high heat capacity. Barium fluoride (BaF_2) is an alkaline-earth element with a wide band gap with many optical applications, such as lithography. BaF_2 has been established as an excellent candidate that is useful for hosting optically active centers (OAC).Lanthanide elements have been used as dopants in BaF_2 lattice to achieve the desired optical properties, which has not been fully explored .With these vast applications of these compounds, it is necessary to carry out complementary theoretical investigations on their properties to explore full applications. The structural, electronic, mechanical and optical properties for LaF_3, BaF_2 and BaF_2:La have been investigated in this current work using theoretical computational modeling. These properties have been studied using the generalized gradient approximation (GGA) employing pseudopotentials and plane wave basis sets as implemented in Density functional theory. Lattice constants and bulk modulus for LaF_3 were calculated and the values obtained were found to be in good agreement with experimental and other theoretical values. Density of states and energy band structure for LaF_3, BaF_2 and BaF_2:La have been obtained along high symmetry points in *k*-space, respectively. A band gap of 7.79eV was obtained for LaF_3 which is an underestimation in comparison to the 9.0eV of experiment. Values of elastic constants calculated for LaF_3 are comparable with those from other experimental and theoretical calculations.LaF_3 exhibits mechanical stability from the obtained elastic constants. Doping BaF_2 with La reduced the band gap and introduced new energy bands within the band gap from the charge compensating fluorine. The elastic constants calculated for BaF_2:La show a decrease in the first two elastic constants with no change in the third component of the elastic constants compared to the pure BaF_2.This has been attributed to the lattice distortion introduced by the La atom. From the defect formation energy calculated, nearest neighbor (NN) formation energy was found to be -26.48eV compared to the next nearest neighbor (NNN) of -27.58e.Itwas observed that the next nearest neighbor is most favorable in BaF_2 lattice. For optical properties, there was a shift in the absorption coefficient from 5.32 m^{-1} to 6.25 m^{-1} of BaF_2 when doped with La. The refractive index of BaF_2 is obtained as 1.52 compared to experimental value of 1.45. The obtained refractive index is in good agreement with experimental values. The introduction of La atom together with the interstitial fluorine affects electronic, mechanical and optical properties of BaF_2.

CHAPTER ONE

INTRODUCTION

1.1 Background to the Study

With the help of supercomputers and high computing resources it has been proved possible to design and analyze novel materials for a specific application (Stefano *et al.*,2013). Experimental studies can be tedious, time consuming, expensive and may not lead to success due to limited resources and equipments. Theoretical modeling through appropriate ‘computing application tools' help us to narrow down on material choices and increase the probability of success in experimental work (Amolo,2018). Through ‘Quantum theory’, the interactions between the constituent atoms of a given material can be determined and this helps to estimate the properties of the material . It becomes indispensable for any ‘Materials Researcher’ to adapt ‘Theoretical Modeling Methods’ in order to predict better potential novel candidate for specific applications. There are many theories and models that have been put forward for a better understanding of the mechanism that accounts for the properties and thereby to design new materials. Band structure calculations have been an effective theoretical tool for researchers in predicting many properties viz., structural, electronic, transport, magnetic, mechanical and physical properties of materials.

Ab-initio quantum methods are computational methods aiming at solving the electronic Schrödinger equation with the knowledge of the positions of nuclei and the number of electrons in the system. *Ab-initio* methods predict the electron densities, energies and other properties of the system (Niu & Mueller, 2016). Density Functional Theory (DFT) is one of those important theories available through the first principles

calculations study. The second chapter discusses in detail about the origin of DFT, the various approximations and methods used in it. This chapter discusses the materials chosen for the present study.

1.2 Lanthanum Fluoride (LaF_3)

Lanthanum fluoride (LaF_3) crystallizes in three major structures i.e. tetragonal, orthorhombic and tysonite phases (Masoud *et al.*,2010).However, the tysonite structure is stable at room temperature and thus suitable for applications at ambient conditions. There is however controversy in their structures since it has been noted that LaF_3 ($P_3\bar{c}1$) and LaF_3 ($P6_3cm$) types are indistinguishable by X-ray diffraction spectroscopy (Crichton *et al.*, 2010).The orthorhombic phase belongs to *Cmma* space group with eight atoms in a primitive cell. From computational method it has been reported that the tetragonal phase exists at high pressure with two formula units per primitive unit cell,*I4/mmm* space group (Winkler *et al.*, 2003). However, in recent studies, trigonal crystal systems are considered as a subset of hexagonal systems. LaF_3 belongs to a group of materials which have several applications. It is used for deep vacuum and ultra-violet (UV) applications because of its high transparency in these wavelengths range which makes a highly refractive layer material (Taki & Muramatsu,2002). LaF_3 is known to be one the materials with the highest ionic conductivities and super-ionic transitions, and it is therefore used as a solid electrolyte in the battery industry (Modak *et al.*, 2009). Its high heat capacity (above 900 K) makes it suitable for applications in electrodes, radiation, fiber optics and fluorescent lamps (Taki & Muramatsu, 2002). Due to the potential of the LaF_3 material for application in vast areas, it is essential to carry out both experimental and theoretical studies on structural and electronic properties of LaF_3.

1.3 Barium Fluoride (BaF_2) and BaF_2:La

Barium fluoride belongs to wide band gap alkaline materials. BaF_2 exists in more than one phase. It exists in a cubic structure whose space group is *Fm3m(C1*) at room temperature conditions. BaF_2 undergoes a phase transition at high pressure of 3-5 GPa to orthorhombic phase space group *Pnma* (C23) .It also becomes hexagonal space group *P63mmc* (B8b) at about 10-15 GPa. Their cubic lattice structure enables transmission of a wide range of wavelengths and indicates independence of absorption from induced polarization. They have similarly matched refractive index values that can be exactly matched to a glass or polymer for use in composite materials (Wang *et al.,* 2005). The cubic fluoride structure also allows for the aggregation and clusters of RE^{3+} ions, making interactions strong and distance between the active ions short (Petit *et al.,* 2006).This implies propensity for ease of energy transfer when the materials are co-doped with RE^{3+} ions. Barium fluoride is found to have transparency in the visible and near-IR regions (Lian *et al.,* 2004). Many theoretical approaches have been employed to study fluoride compounds at the excited states or ground state. Figure 1.1illustrates the structure of cubic BaF_2 at ambient condition, (Fooladchang *et al.,* 2013).

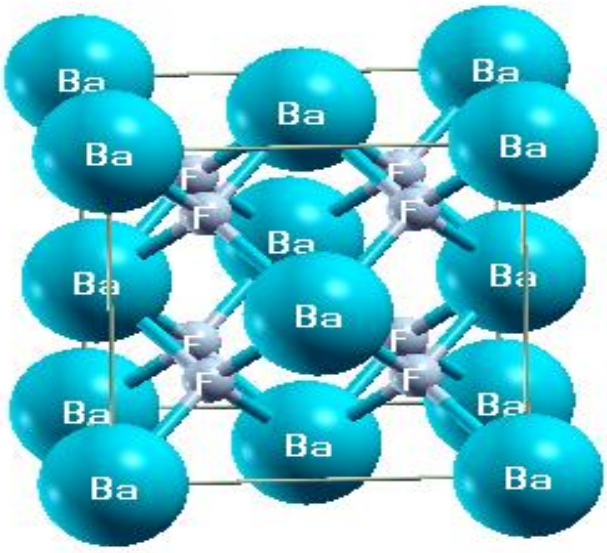

Figure1. 1: Cubic structure of BaF_2

Barium fluoride (BaF_2) belongs to alkaline-earth elements with large band gaps which are applicable in many optical applications, (Nyawere *et al.*, 2014).As an example in lithography application, BaF_2 is used as a lens material because of its short wavelength (Shi *et al.,* 2011).The introduction of an interface that makes the ions to be redistributed in the space charge region in BaF_2 makes it to be considered as a superionic conductivity material. This can also be done by appropriate impurities being dissolved into the lattice, and therefore BaF_2 is considered as a candidate material for high-temperature batteries, fuel cells, chemical filters and sensors (Sata *et al.,* 2000).Solids with superionic conductivity properties allow ions to move through the structure macroscopically making the material to posses ionic conductivity at high levels while in the solid state, (Keen *et al.*, 2002). They are also regarded to be fast ion conductors with negligible electronic conductivity.

Due to lanthanides contraction it has been established that the radii of rare-earth ions decrease with increasing atomic number (Chen *et al.*, 2008). The structure of the external electron orbitals of these ions remain practically unchanged, because the electrons are filling the localized 4f shell at the same time. Fluorite structure materials, can be disordered by introducing trivalent elements for example the lanthanides or by thermal activation (intrinsic conductors), making these structures good examples for studies of the mechanism of ionic transport in crystalline materials.

It has been established that in any real material the unavoidably presence of impurities and defects strongly affects both mechanical and optical properties of their crystals, (Huang *et al.*, 2016). BaF_2 has been established as an excellent candidate that is useful for hosting optically active centers (OAC) and lanthanide elements used as dopants in BaF_2 lattice to achieve the desired optical properties. Understanding the electronic and mechanical properties of BaF_2 and BaF_2:La is considered of great importance in the search for new materials applicable in areas such as solid electrolytes which has potential application in the battery industry among other applications.

1.4 Statement of the Problem

LaF_3 is a model system for several applications. From recent literature, discrepancies between experimental data and computational results obtained for structural and electronic properties still exist. BaF_2 exhibits superionic conductivity, it has been reported that this property can be improved by doping it with rare earth ions. This superionic property enables BaF_2 to be regarded as a candidate material for high-temperature batteries, fuel cells, chemical filters and sensors (Sata *et al.*, 2000).

1.5 General objective

To determine the structural, electronic and mechanical properties of LaF_3 and BaF_2:La at ground state.

1.6 Specific objectives

i. To determine structural and electronic properties of LaF_3 and BaF_2:La

ii. To determine the elastic constants of LaF_3 and BaF_2:La using *ab initio* method with Density Functional Theory as implemented in the Quantum Espresso Code.

iii. To study the interstitial defect formation energy in La doped BaF_2.

iv. To study the optical properties of BaF_2 and BaF_2: La .

1.7 Significance of the Study/Justification

A super-ionic transition exists in Lanthanum compounds and especially in LaF_3 compound. It is this property that makes LaF_3 appropriate for use as a solid electrolyte which has potential application in the battery industry. This material has unusual high heat capacity (above 900 K), suitable for application in high temperature electrodes. On the other hand, BaF_2 is a wide band gap material whose band gap decreases when doped with lanthanum. The doping substantially increases its conductivity through reduced band gap (Labeguerie *et al.,* 2006). Trial and error in some experimental methods have been used to carry out doping and the current results are expected to enable experimentalists give an optimum application of BaF_2:La.

1.8 Scope of the Study

Structural, electronic and mechanical properties of the tysonite phase of LaF_3 using first principles method are here studied. This thesis also presents results from the study of electronic, mechanical and optical properties of lanthanum doped barium fluoride (BaF_2:La) supercell. The consequences of La as an impurity on optical properties of BaF_2 and mechanical properties of BaF_2:La have also been studied. The defect formation energy is also discussed. This thesis is arranged in the following order; Chapter 1 is the introduction on LaF_3, BaF_2 and BaF_2:La materials with their applications. Chapter 2 gives a detailed account on the works done by other scholars on $LaF_3$and BaF_2:La. Chapters 3 gives detailed methodology of the research. Chapter 4 gives the results and discussion with comparison with previous studies done this far. Chapter 5 provides conclusive remarks, recommendations on the study and the gaps to be filled in future.

CHAPTER TWO

LITERATURE REVIEW

2.1 Introduction

Computational methods are solving problems in material design because of their capability to examine and control material invention with newest complexity, (Knauth & Tuller, 2002). Computer simulations in atomic designs have played major roles in illustrating relevant energetic and structural properties of atoms that makes up materials. Designing and simulation of materials using computers includes various disciplines such as statistical mechanics and quantum chemistry and solid state physics. A good understanding of the concepts underlying the computer simulation approaches have major impacts on strengths and disadvantages for material designers to benefit fully from the computational methods while illuminating the doubts that are associated with the methods. Computer simulations have been used to interrogate a vast range of materials such as graphite among others and magnetic materials (Makau *et al.,* 2006). The results obtained from these investigations are comparable to experimental results and the approaches used here are therefore encouraged in the search of new materials, (Knauth & Tuller,2002).

2.2 Lanthanum Fluoride (LaF_3)

Electronic and structural properties of LaF_3have been studied widely through experimental (Crichton *et al.,* 2010) and theoretical methods (Modak *et al.,* 2009). Experimentally, it has been established that at about 20GPa the trigonal structure of LaF_3 transits into a new phase structure, as studied by X-ray diffraction method, (Crichton *et al.,* 2010). A new orthorhombic phase that belongs to *Cmma* space group with eight formulas in a unit cell (Dyuzhena *et al.,* 2003) is formed. In parameter-free

atomistic model simulations, synchrotron X-ray diffraction and Raman spectroscopy it predicts the occurrence of orthorhombic phase with space group *Pmmn* and that this phase remains stable up to 60 GPa this is according to Crichton, (Crichton *et al.,* 2010). Zhenlong and the co-author shave used the plane -wave pseudo-potential density functional method, as implemented in Castep in the study of elastic constants, thermodynamic and electronic properties of LaF_3 in tysonite structure (Zhenlong *et al.,* 2014). LaF_3 was established to have a wide-band-gap of 7.74 eV, though this results on band gaps are very exact compared with experimental results obtained earlier of 9.7eV.Other methods such as full potential linearized augmented plane wave (FP_LAPW) method as implemented in WIEN2K have been explored in the study of band gaps in LaF_3 and reported a band gap of 6eV lower than experimental work of Modak and others (Modak *et al.,* 2009). However, this has brought a disagreement with the tysonite phase which has not been studied extensively. This is due to the fact that the tysonite structure is complex compared to others in existence and studied this far.

LaF_3 has also been studied by use of the first-principles VASP code approach. Results reported that tysonite structure transforms to a primitive orthorhombic structure (*Pmmn*) at around <19.5GPa, these results are not comparable with the experimental of 16 Gpa. (Sahoo *et al.,* 2017). Though various studies have been done on LaF_3, there exist some controversy in terms of exact results obtained between the experimental methods and computational simulations. Rare earth elements have been used as dopants in various materials, as defined by respective application. For instance, when doped in glasses they allow for broader emission and absorption spectral properties (with respect to crystalline hosts), making them ideal for many optical fiber devices

such as lenses. Other applications require crystalline hosts for their inherently superior, thermal properties and narrower line-widths (Joubert *et al.,* 2005).

LaF_3 also exhibits superionic property. Superionic conductors represent a group of materials which show anomalous high ionic conductivity. The macroscopically allowed movement of ions in materials is characterized by strong disorder in their lattice and leads to exceptionally high (liquid-like) values of ionic conductivity whilst in the solid state. The behavior particularly happens at higher temperatures which are featured with a very fast diffusion of larger fraction constituting of different species within an essentially rigid framework formed by the species (Keen *et al.,* 2002). Mixed conductors are some of the materials, which are good electronic conductors, while ionic conductors refer to superionic conductors or fast ion conductors with almost zero electronic conductivity, which are sometimes called solid electrolytes and often used in electronic devices. Fast conductors or solid electrolytes have continuously given rise to interest in their high ionic mobility, in many technological promises and as solid state materials for the research of various problems. The fast conductor materials have been equated to higher levels of ionic conductivities; they also exhibit various different types of characteristics both in the critical region and in the fast ion state. As a result of drifting of ions, ionic crystals possess small electrical conductivity. Compared to liquid phase the superionic conductors have smaller drifts, this makes the ions capable of diffusing from one site to another within the lattice. The thermally created lattice defects results into these drifts. At temperatures just below melting point, T_m, the fluorites exhibit broad specific heat anomaly which passes through a maximum at a particular temperature, T_c. Ionic conductivity increases with temperature which in turn is increased by the presence of Schottky

defects. This is where vacancy allows other atoms to easily diffuse through it since less energy is required to move the electrons and in the process, vacancy migrates in opposite direction. This migration is referred to as diffusion and it is an important property which helps understand if it is likely that the defect can be incorporated during growth and processing. This also helps in the understanding of impurity diffusion, which is always mediated by original defects (Limpijumnong & Van de Walle, 2004). Diffusion is a key aspect in mechanism of device degradation and increases electrical conduction. For proper interpretation of results and comparison with experiments, it is necessary to have knowledge of defect formation energy.

Materials that contain large numbers of defects, so that the ions can migrate easily (at high temperature) can have a high ionic conductivity, (Wang *et al.,* 2006). In some ionic materials, this high ionic conductivity with liquid-like values is attained before the melting of the crystal and such materials are also known as superionic conductors. Superionic conduction can occur through distortion of lattice structure at the lower temperatures. Structure of materials makes it an ordinary ionic crystal, but at elevated temperatures it undergoes a non-continuous change to new structure in which the conductivity is liquid-like. The materials can also change to superionic as a result of change in defect concentration becoming larger before melting point. Fluorite compounds that undergo diffusion that is a continuous transition are being accepted at high temperature to other states that are heavy and less massive dynamic disorder in the sub-lattice of anion and transport of ions are through a hopping mechanism. The clarification of some of the conduction mechanisms and other aspects of fast conductors such as defect structure, the extent and exact nature of disorder are still not well explored.

LaF_3 has superionic transitions and ionic conductivity (Sinitsyn *et al.,* 2003). Ionic superconductivity finds many applications as a solid electrolyte and may soon be used in the battery industry. Electrical conduction in the ionic state is majorly through the F^-ion since La^{3+} is heavy and cannot easily move through vacancies in the crystal as F^-. It is important to note that LaF_3 is essentially but not purely ionic (Sinitsyn *et al.,* 2003) since there are very small covalent bonds between La and F. This is the major reason for different conclusions about parameters of LaF_3 crystal from different atomic simulation studies depending on quantum or chemical charges used.

Regardless of type of parameters used, the final characteristics of luminescent devices are dependent upon the optical properties resulting from the ion-host interactions. For increase in efficiency of a given device, excitation efficiency needs to be increased. The quantum efficiency of a material system is given as a ratio of the emitted to absorbed photons and varies between 0 to 1.The vibrational energy of the host material is lower if the non-radiative contribution to electron decay is less, which ultimately increases the quantum efficiency. Therefore, choosing a host material is an important step in the fabrication of optical devices.

Fluorides emerge at an upper hand as host materials due to their low intrinsic vibrational energies which extend transmission to the far ultraviolet and infrared spectral regimes in luminescent materials (Wang *et al.,* 2006). The interaction between rare earth (RE) ions and host material is important, as well as the luminescent efficiency of the materials. Lanthanum tri-fluoride, LaF_3, is a very suitable host because the RE^{3+} can easily substitute for the La^{3+} of the same valence, (Chen *et al.,* 2008). The vibrational energy of LaF_3 is reported to be ~350cm^{-1}, has a high RE

solubility with significant environmental and thermal stability. Ground state has been established to be the corner stone for comprehension of the important properties of materials which provides important knowledge for material applications.

2.3 BaF_2 and BaF_2:La

It has been established in various studies that the electronic structure of BaF_2 crystals differs from that of other alkaline-earth fluorides in that BaF_2 has an energy gap between the occupied states of the anion and cation: which is less than one-half of the main band gaps, (Kuznetsov *et al.,* 2003). It is due to this energy gap that BaF_2 is a fast scintillator making it the most studied alkaline earth fluoride. Although BaF_2 suffers from slow luminescence, it has been established that this can be improved by doping it with rare earth elements such as La, (Nepomnyashikh *et al.,* 2001).

Fluorite structures may be disarranged either by thermal activation (intrinsic conductors) or by doping with trivalents (extrinsic conductors) for example lanthanides. Therefore, these crystals become perfect candidates for investigation of the mechanism of ionic transport in crystalline materials. Lanthanide elements are generally defined as those in which the 4f orbitals are progressively filled. Current notable commercial use of lanthanides is in electrodes of batteries of hybrid vehicles. Other lanthanides such as, cerium (the most abundant of the rare earth elements) are most notably known for their use in catalytic converters; Europium (as well as Terbium) is widely used as a phosphor in color television tubes and has more recently been used as an anti-counterfeiting phosphor in the European Union's paper currency; (Sata *et al.,* 2000).

Calcium fluoride, strontium fluoride and barium fluoride are alkaline earth elements that possess similar characteristics and have been studied for various properties. Their cubic lattice structure enables transmission for a wide range of wavelengths and as well indicates independence of absorption from induced polarization. The cubic fluoride structure also allows for the aggregation and clusters of RE^{3+} ions, making interactions strong and distance between the active ions short (Petit *et al.,* 2006), implying a propensity for ease of energy transfer when the materials are co-doped with differing RE^{3+} ions. Barium fluoride, BaF_2, is found to have transparency in the visible and near-IR region, (Lian *et al.,* 2004). In addition, BaF_2 has slight solubility in water and is non-hygroscopic, and due to its cubic structure, has one refractive index which can be exactly matched to that of glass or polymer matrix material to avoid significant light scattering, making it desirable for use as composites.

Lanthanum is the most effectively used dopant in BaF_2 and it improves characteristics of BaF_2 including; mechanical strength, radiation, resistance and density. It has been established that BaF_2 exhibits high superionic conductivity through incorporating of appropriate impurities into the lattice or the introduction of an interface that causes the redistribution of ions in the space charge region, (Sata *et al.,* 2000). The incorporation of lanthanum affects the valence band of barium fluoride where extra states can be created in the band structure, (Nepomnyashikh *et al.,* 2001). These effects can be studied through computational methods. The electronic structural properties of La doped BaF_2 were studied by periodic density functional theory (DFT) calculations as implemented in linear combination of atomic orbitals (LCAO) approximation. LCAO–DFT approximation involves the linear combination of the Gaussian orbitals and were employed in the construct of the localized atomic basis,

which then constructed the Bloch functions by combining linearly with the plane-wave phase factors. The calculations based on this framework were noted to provide good description of electronic excitation properties though the approach is not reliable in describing the band structure of BaF_2 and other materials.

Experimentally, CaF_2, SrF_2, BaF_2, density of states for intra-band transitions were studied by photoelectron spectrometry (Garcia *et al.,* 2005). The laser absorption spectra techniques were used to analyze the impact of Eu defects on β-PbF_2 (PbF_2:Eu^{3+})versus the electronic excitation spectra and dielectric relaxation (Labeguerie *et al.,* 2006). The mixture of β-PbF_2 and CdF_2 crystals absorption coefficients were reported by spectrophotometry measurements. However, experimental results obtained on the electronic structure of BaF_2:La are still not in agreement with some theoretical results because of the errors involved in these calculations.

2.4 Structural and Electronic Properties Calculations

Interaction of electrons with atomic cores affects both the physical and chemical properties of a system. The treatment of electron-electron interactions is the major source of difficulty in the interpretation of these properties since the interactions are inseparable or treated without approximation. Schrödinger equations well solved for a specific system can be differentiated from one to other forms of modeling approaches since they are majorly *ab-initio* in nature (Giannozzi *et al.,* 2001). The solution of Schrödinger equations remains a difficult task. Exact solutions of the equation, in general, can only be solved if time is scaling exponentially with system size (Giannozzi *et al.,* 2001). This scaling precludes exact calculations for all but the

smallest and simplest of systems e.g., the hydrogen atom. The degree of accuracy and the predictive power can be lost by the introduction of approximations which may be used to reduce the equations to a form that can be solved.

The density functional theory (DFT) and computer simulation methods involved in various solving of the Schrödinger equations have become more successful in calculations involving electronic structure properties and other material properties applicable to several systems relevant to the real world. In general, the density functional and quantum chemical among other approaches that involve approximations for the electron-electron interactions have been reported to limiting the achievable accuracy in the calculations involved.

2.5 Elastic constants for LaF_3

Elastic constants majorly define mechanical and dynamical characteristics, especially the stability and the stiffness of a material (Nyawere *et al.*, 2014). These parameters are sources of probing inter-atomic forces. Although LaF_3 belongs to the tysonite structure, its mechanical properties were calculated within the hexagonal phase group of crystals (Sin'ko & Smirnow, 2002). The elastic constants of LaF_3 have been examined both experimentally and theoretically. Diniz and Paschoal obtained the elastic constants of LaF_3 at 0 GPa using the shell-model method. Although the results presented were comparable to the experimental work they had a big difference compared to experimental results obtained earlier (Diniz & Paschol, 2007). Unfortunately, these results are not the exact representation of the elastic constants for C_{14}. LaF_3 is categorized to have a trigonal structure but the elastic constants were obtained in the hexagonal symmetry framework (Benner, 2002). Zhenlong also

calculated the elastic constants of LaF_3 using CASTEP approach in DFT and the results were compared to the experimental results. On further calculations it was reported that at 0 GPa elastic constants for LaF_3met mechanical stability requirements for the trigonal crystal (Zhenlong *et al.*, 2014).

2.5.1 Elastic constants for BaF_2 and BaF_2:La

Barium fluoride (BaF_2) is an ionic crystal in the class of fluorites with a structure that consists of three transversing face centered cubic lattices (Lian *et al.*, 2004). The calculations of the elastic constants for barium fluoride were focused on anon-polarizable model of non-flexible ions and predicted only part of the experimental C_{12}-C_{44}. This non-flexible (rigid ion) model did not explain clearly the relationship between the optical, dielectric and dispersion relations of some other ionic crystal. The shell model approach by Sobolev and others was introduced for the explanation of the dielectric constants in BaF_2:La and it acknowledged the ionic polarization (Sobolev *et al.*, 2002) and thereafter it extends the incorporation of vibrational spectrum entirely. Elastic constants of BaF_2 have so far been studied in its cubic (most stable), orthorhombic and hexagonal phases using quantum espresso; results obtained were comparable with experimental and other theoretical results, (Nyawere *et al.*, 2014).

In doped and pure fluorite structures, the calculation of elastic constants has provided important information. There are various models used to determine the elastic constant of BaF_2 and its dopants. Diffuse super-ionic transition temperature T_c is as a result of reduced anion-Frenkel defect formation energy, which is caused by their binding energy.

An analogous model has been suggested for substitutional trivalent cations doped with fluorites (Dubinin *et al.*, 2004). This model involves the impurity-stabilised clusters which are meant to bind interstitials resulting to a reduced T_c, while increasing the concentration of the dopant. Calculations in static lattices show that changes inelastic constants in some doped fluorites, specifically a decrease in C_{I1}, are expected with anion Frenkel disorder. The results of T_c achieved from these measurements are comparable with other methods. The elastic constants for BaF_2:La has been studied (Dubinin *et al.,* 2004) and the achieved results for C_{44} have shown unusual behavior with the first region having the same slope to that of the pure crystal then followed by a decrease in linear region. From these results, an indication of a decrease in C_{ll} and C_{44} which was part of the same process was noted. The fact that C_{44}, in Ba and LaF_3 also underwent a decrease is significant. These results have been compared in this work.

2.6 Defects and Defect Formation Energy

Theoretical study of these defects has been done successfully in BaF_2, (Nyawere *et al.,* 2014). Fluorides belong to a very special class of compounds with interesting physical properties, crystallizing in a variety of structures, with many applications such as optical coatings among many other technological applications(Morris *et al.,* 2001). Properties, such as crystallization in the fluoride structure has been explored widely although a few questions regarding the structure-property relationships are still being raised.

It has since been established that doping of BaF_2 with La increases its performance as a material in its various applications but the physics behind this is still not yet clear. Experimental and theoretical attempts regarding the investigation of the properties of BaF_2:La has been done. Calculations have been carried out on formation energy and the structure of BaF_2:La for the equilibrium positions of nearest neighbor (NN) and next nearest neighbor (NNN) complexes have been achieved through molecular statics (MS) approach, (Sobolev *et al.,* 2002). The result obtained in MS methods has a basis of various forms of the ion–ion interaction description. The band structure and density of states (DOS) calculations for BaF_2:La crystals for the NNN structure was achieved through minimizing of the total energy. The La^{3+} impurity introduced in BaF_2 results in the appearance of the fluorine interstitial, (F_i) of the 2p state is linked to the upper electronic band (Sobolev *et al.,* 2002).

2.7 Optical properties of BaF_2 and BaF_2:La

Rare earths are used as dopants in various materials, as defined by the application such as in barium fluoride. Regardless of the type of use, the final characteristics of luminescent devices are dependent upon the optical properties resulting from the ion-host interactions. Fluorides emerge as advantageous host materials due to their low intrinsic vibrational energies which extend transmission to the far ultra-violet and infrared spectral regimes. This minimally quenches the excited state of rare earth ions and has high transparency over a wide wavelength range. It also has high ionicity and fundamentally reduced absorption when compared to oxide based materials, (Garcia *et al.,* 2003). Lanthanum tri-fluoride, LaF_3, is a very suitable host material because the RE^{3+} can easily substitute for the La^{3+} of the same valence (Chen *et al.,* 2008). The cubic fluoride structure also allows for the aggregation and clusters of RE^{3+} ions

which makes the distance between the active ions short and interactions strong (Petit *et al.*, 2006), implying a propensity for ease of energy transfer when the materials are doped.

CHAPTER THREE

MATERIALS AND METHODS

3.1 Introduction

Most materials are termed as solid state materials which can be described as many-body systems consisting of electrons and nuclei which are interacting electromagnetically. Quantum many body problems are reduced to interactions of electron systems with the movement of the potential of the nuclei at fixed positions, this is referred to as first-principles method (Burke *et al.,* 2007).Density functional theory is among the common methods where the electronic structure calculations are done at ground state in quantum chemistry and solid state physics (Clark *et al.,* 2005). This theory gives solutions to the Schrödinger equation for many-body or many-electron systems as a function of charge density, rather than solving the wave-function. In many-electron (many-body) systems, the exchange-correlation also termed as self-interactions relations, cause electrons to be indistinguishable, leading to the fact that energy and forces are impossible to be solved analytically. DFT provides a balance between computational cost and accuracy that allows quantitative data to be computed for any material model (up to thousands of atoms) (Clark *et al.,* 2005). Therefore, the computational work based on DFT is well suited to a variety of material science applications such as surface science and catalysis, structural metals and earth sciences, (Kang *et al.,* 2002).

The aim of the first-principles method is to come up with a solution to the Schrödinger time-independent, non-relativistic equation. This equation for such systems is given as:

$$H\varphi_k(r_1\sigma_1.....,r_N\sigma_N) = E_k\varphi_k(r_1\sigma_1.....,r_N\sigma_N) \qquad (3.1)$$

where total Hamiltonian *H* is;

$$H = -\sum_i \frac{\hbar^2}{2m}\nabla_i^2 + \frac{1}{2}\sum_{i\neq j}\frac{e^2}{\left|\mathbf{r}_i - \mathbf{r}_j\right|} - \sum_{i,j}\frac{Z_1 e}{\left|\mathbf{r}_i - \mathbf{R}_j\right|} - \sum_1 \frac{\hbar^2}{2M_1}\nabla_1^2 + \frac{1}{2}\sum_{I\neq J}\frac{Z_1 Z_J}{\left|\mathbf{R}_I - R_J\right|} \qquad (3.2)$$

where ψ is the full wavefunction for all the particles in interaction (electrons, nuclei and electromagnetic field). E_k is the corresponding energy to the wavefunction ψ and they obey Pauli Exclusion Principle. In equation, (3.2), the first, second and third terms represent kinetic energy of the electrons, the electron-electron Coulomb interaction and the electron-nuclei interaction respectively. The fourth term is nuclei kinetic energy and the last term is the nucleus-nucleus interaction. The symbols $\vec{r_i}$ is the electron position, $\overrightarrow{R_i}$ refers to nuclei positions, *m* is the electron mass, *e* electron charge, M_I are the nuclei masses, Z_I nuclei charges and $\hbar$ is the reduced Plank constant.

The Born-Oppenheimer approximation (Cottenier, 2013) assumes that the nuclei are much heavier when compared to those of electrons and hence should be much slower. Hence, they can be relatively considered to be "frozen" or at rest in fixed positions. Hence one could also assume that the electrons are in equilibrium to the nuclei at every instant. This approximation solves the problem with an assumption that the nuclei is much heavier compared to electrons that are lighter and therefore will their movement is slower, then the electronic and nuclear motion are easily separated. Nuclei are treated to be stationary and the electrons move relative to them. Equation (3.1), can be separated into two independent eigenvalue problems such that the electron and nuclei wave functions are products of the total wave function

$$\varphi(\vec{r}, \vec{R}) = \psi_e(\vec{r}, \vec{R}) \times \psi_{nucl}(\vec{R}) \qquad (3.3)$$

And the electron wave function depends on the nucleus co-ordinates. Given that the nuclei are now treated to be stationary, we neglect the nuclei problem since it can be incorporated later. The Hamiltonian in eqn. (3.3) can be written as:

$$\boldsymbol{H} = \boldsymbol{T}_e + \boldsymbol{V}_{en} + \boldsymbol{T}_n + \boldsymbol{V}_{nn} \qquad (3.4)$$

3.2 Hohenberg-Kohn Theorems

The foundation of density functional theory was laid by Hohenberg and Kohn (HK) (Hohenberg & Kohn, 1964) in 1964. They established a direct relationship between the potential $v(\vec{r})$ and electron density $n(\vec{r})$ at ground state, in such a way that the infinitely complex many-body problem of solving the Schrödinger equation for N particles can be replaced by an equation for the density $n(\vec{r})$. According to Hohenberg and Kohn, it is not possible for a system with electrons to produce similar ground-state electronic charge density $n(\vec{r})$when two different potentials act upon them. The total Hamiltonian for this many-body is implied by $n(\vec{r})$. Hence all the excited states and their energies are also implied by $n(\vec{r})$. Hohenberg-Kohn theorem therefore confirms that by using $n(\vec{r})$ rather than wave-functions the details of many-body Physics can be understood (Giovanni, *et al.*,1996). Hohenberg-Kohn also showed that a universal functional $F\ [n(\vec{r})]$ exists and it is an electron density $n(\vec{r})$ functional whose actual energy ground state at $E\ [n(\vec{r})]$ is given by:

$$E[n(\vec{r})] = F[n(\vec{r})] + \int n(\vec{r}) V_{ext}(\vec{r}) d^3\tau \qquad (3.5)$$

The energy $E[n((\vec{r}))]$ is minimized under the constraint that the integral $n(\overrightarrow{r})$ is equivalent to the sum of electrons. The minimum value coincides with energy at ground-state. Hence based on these theorems, the Hamiltonian value expected in eqn. (3.5) is written as

$$\langle \varphi | H | \varphi \rangle = E[n(\vec{r})] \tag{3.6}$$

where $E[n(\vec{r})]$ is total energy functional at ground state and $n(\vec{r})$ is the electron density. Once the correct density is known, it therefore follows that the properties of the system can be calculated at the ground state. The energy functional is minimized to calculate the ground state density correctly:

$$E_{\mathrm{o}} = \frac{\delta}{\delta n} E[n(\vec{r})] = E[n_{\mathrm{o}}(r)] \tag{3.7}$$

Equation (3.7) gives the basis foundation of density-functional theory (Parr & Yang, 1995). This allows large simplifying of concepts in the quantum-mechanical problem in search of ground state properties for a system interacting with electrons. This replaces the ordinary description based on wave functions (which depend on 3N independent variables, *N* being the number of electrons) with one which depends only on three variables and charge density. However, there are two major impediments to straight forward application of this theorem. The first form of the *F* functional is the unknown and the second requirement is fulfilled if the function $n(\vec{r})$ is to be considered an acceptable ground-state charge distribution (and hence the domain of the functional (*F*) is poorly characterized. The second part of the problem is never considered but Lagrange multipliers are used for normalization of the charge density effectively. The first part of the problem was addressed by Kohn and Sham (Kohn & Sham *et al.,* 1965) as discussed below.

3.3 Kohn-Sham Approach E_{xc}

This approach proposed an approximated functional in many body electron systems because the functional F[n] was not practical. It involved an auxiliary system of non-interacting electrons moving in an external potential V_{KS} whose ground state

electron density was similar to that of real electron system interaction. The kinetic energy of the system and the electron density were exactly known from the orbital. The universal functional for a non-interacting system is given by;

$$F[n(r)] = T_s[n(r)] = \langle \varphi_{ks} | T | \varphi_{ks} \rangle \tag{3.8}$$

Total energy functional is denoted as:

$$E_{ks}[n(r)] = \min T_s[n(r)] + \int V_{ks}(r) n(r) dr - \mu' \left[\int n(r) d^3 r - N \right] \tag{3.9}$$

μ' is the Lagrange multiplier that ensures the conservation of the number of electrons. The V_{KS} function can be obtained as follows:

From the interacting system, the universal functional is written as;

$$F[n(r)] = T_s[n(r)] + E_H[n(r)] + E_{xc}[n(r)] \tag{3.10}$$

At ground state:

$$0 = \frac{dE_{Gs}}{dn} = \frac{dT_s}{dn} + V_H n(r) + V_{xc}[r] + V_{ext}(r) - \mu \tag{3.11}$$

Similarly, for auxiliary system, at ground state:

$$0 = \frac{dE_{Gs}}{dn} = \frac{dT_s}{dn} + V_{ks}(r) \pm \mu' \tag{3.12}$$

From the two equations the potential $V_{ks}(r)$ can be obtained

$$V_{ks}(r) = +V_H n(r) + V_{xc}(r) + V_{ext}(r) \tag{3.13}$$

The self-consistent (Kohn-Sham)equations can be expressed as;

$$\left(\frac{-\hbar \nabla^2}{2m} + V_{ks}(r) \right) \varphi_{ks}(r) = \varepsilon_k \varphi_{ks}(r) \tag{3.14}$$

$$V_{ks}(r) = +V_H n(r) + V_{xc}(r) + V_{ext}(r) \tag{3.15}$$

$$n(r) = \sum_{iEcc} |\varphi_{iks}(r)|^2 \tag{3.16}$$

where $\epsilon_\kappa$is Lagrange multiplier for normalization. $v_{eff}(\vec{r})$ contains external potential, Hartree energy (electrostatic energy) and exchange-correlation. The exchange-correlation potential is defined as;

$$V_{xc}(r) = \int \frac{n(r)}{|r - r'|} dr' \tag{3.17}$$

$$V_{xc}(r) = \frac{\delta E_{xc}(n(r))}{\delta n(r)} \tag{3.18}$$

All equations from Kohn-Sham are solved self-consistently. The flow chart, in figure 3.1 illustrates a clear computational procedure for any DFT-based calculation

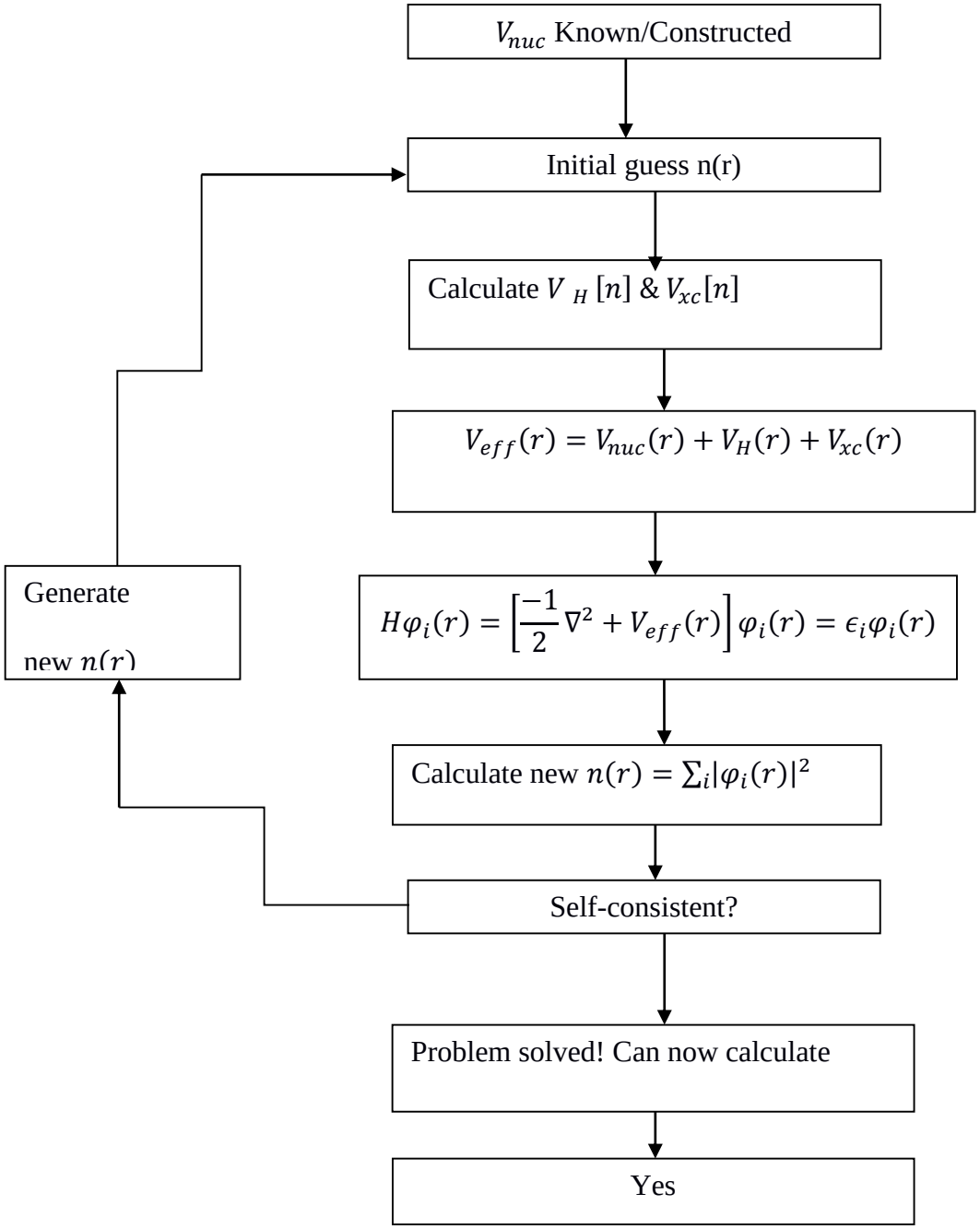

Figure 3.1: A typical computational procedure

The procedure requires an input, which is a geometrical arrangement of atoms determining the overall atomic potential v(r), and the atomic number Z. It begins with a guess at the start for the electron charge density, the exchange-correlation potential and the Hartree potential are then calculated from it (Payne *et al.*,1992). A typical

self-consistency is achieved when the generated charge density is smaller than the chosen values, (Payne *et al.*,1992). Minimum energy is then obtained from the electronic charge density n(r)which gives the minimum energy guessed. The density which is a function of *r* is computed and then used as another function for computing the Hartree potential and the exchange-correlation potential. The result of$V_H\,(r), V_{xc}(r)$and $V_{nuc}\,(r)$ gives the effective potential $V_{eff}\,(r)$

Therefore, the Hamiltonian of the system is equal to$V_{eff}\,(r)$ + K.E that is:

$$H\varphi_i(r)=\left[\frac{-\hbar^2\nabla^2}{2}+V_{eff}(r)\right]\varphi_i(r)=\varepsilon_i\varphi_i(r) \tag{3.19}$$

where ϵ_i is the minimum energy.

3.4 The exchange correlation functionals

Once the Kohn-Sham equation is obtained, computing of each part of DFT energy becomes easy, except for the "exchange-correlation". This complicated exchange correlation energy functional can be obtained through various approximations

3.4.1 Local Density Approximations (LDA)

This is one of the easiest and the founder of all the other approximations. The fundamental concept is the application of the exact exchange-correlation energies of the homogeneous electron gas as an approximation to the energies of inhomogeneous systems. The approach incorporates an exchange-correlation functional E_{xc}^{LDA} written in the form:

$$E_{xc}^{LDA}=\int n(\vec{r})\varepsilon_{xc}^{\hom}(n(\vec{r}))dr \tag{3.20}$$

$\in_{xc}^{hom}$ is the exchange-correlation energy per particle of a homogeneous electron gas with density $n(r)$.Defining $E_{xc}^{LDA}[n(r)]$ allows the calculation of the exchange-correlation potential involved in this method.

3.4.2 Shortcomings and Improvements of LDA

LDA has a good performance so far in the calculations taken, however its limitation should be put in consideration especially in applications. It performs well in systems with slow ratio in density and their chemical properties are well produced.LDA is however not accurate in systems that have independent particle that tend to break down. In transition metal oxides XO (X=Fe, Mn, Ni) for instance, which belong to Mott insulators, they are perceived to be semiconductors or metals by LDA.

LDA also gets the ground state for many simpler cases wrongly. For example, the titanium atom ground state properties are wrongly predicted using LDA approach. The van der Waals are not considered in LDA which makes the hydrogen bonding wrongly described, yet in Biochemistry bonding is very important and this has led to a lot of discrepancies in theoretical and experimental data. This is particular in the DNA structure which depends solely on hydrogen bonding. LDA can be improved by the inclusion of gradient corrections that makes up a functional comprising of the density and its gradient referred to as the generalized gradient approximation (GGA).Although LDA has worked excellently for several systems sometimes it is necessary to use other functions. There are many attempts to go beyond LDA by expanding the exchange-correlation functional in a series of power including higher order terms.

3.4.3 Generalized Gradient Approximation (GGA)

This method is a continuation of LDA where it takes in account both the density of uniform electron gas and its deviation from homogeneity by considering the gradient of charge densities. This exchange-correlation energy is written in the form:

$$E_{xc}^{GGA} = \int \varepsilon_{xc} n(r) \nabla n(r) dr \tag{3.21}$$

The GGA exchange correlation potential is written as:

$$V_{xc}(r) = \frac{dE_{xcG}}{dn(r)} = \frac{+dF_{xc}}{dn} - \sum_{\alpha=1}^{3} d \propto \left(\frac{dF_{xc}}{d(d\alpha n)} \right) / n = n(r) \tag{3.22}$$

where $F_{xc}(n, |\nabla n|) = E_{xc}(n, \nabla)n$, $\partial\alpha$ stands for gradient component GGA improved significantly the LDA's description of the binding energies of real systems. However, both LDA and GGA have a limitation in describing the correct electronic properties of some classes of materials for instance in the transition metal oxides and strongly correlated systems.

3.4.4 Hybrid functionals and GW approximation

Semiconductors are vital technological materials with numerous applications and to obtain first principles approaches that can give and illustrate their properties accurately is very important. It has been established that band gaps obtained by both LDA and GGA are underestimated for semiconductors, while the Hatree-Fock methods overestimates their band gaps. It has been proposed that these challenges in band gaps can be overcome by use of Hybrid functionals. This was done by obtaining suitable functionals through suitable mixture of the local or semi-local DFT exchange energy functionals and the non-local Hartree-Fock exchange energies. HSE06 functionals have been proposed to solve the band gaps challenges (Paier *et al.*, 2006).

3.5 Implementation

3.5.1 Plane waves

The Born-Oppenheimer approximation and density functional theory have been used as a link between the nuclei and electrons interactions commonly known as many body problem and the single particle problem moving with an effective potential for a set of stationary nuclei. The common approach is used when the single particle eigenstates is expanded into a basis set of plane waves. The use of plane waves is due to the fact that the eigenstates are termed to be the exact of the homogeneous electron gas and are not specified to any particular atom. The plane-waves expansion of the Kohn-Sham wave function is important in the total energy calculations of solids and it is periodic. Now the solutions of this single-particle Schrödinger equation with a periodic potential, is itself periodic and obeys the Bloch's theorem.

$$\varphi_{kj}(r) = \mu_{kj}(r) e^{(i\vec{k}r)} \tag{3.23}$$

k is the crystal momentum and *j* the band index classifies the electronic states with same **k**-vector and these **k**-vectors are defined within the first Brillion Zone.$u_{kj}(\boldsymbol{r})$ has the periodicity of the crystal which can be solved using a basis set.

$$\varphi_{kj}(r) = \sum_{G} C_j, G + k e^{i(K+G),r} \tag{3.24}$$

G is defined by the equation G. b= 2πm, b are the lattice vectors of the crystal and m is an integer. Therefore the expansion leads to

$$\varphi_{kj}(r) = \sum_{G} cj, K + G e^{ikr} \mu_{kj}(r) \tag{3.25}$$

Using the Bloch states, the Kohn-Sham equation becomes:

$$\left[\frac{-\hbar}{2m}\nabla^2 + V_{eff}(r)\right]\varphi_{kj}(r) = \varepsilon_{kj}\varphi_{kj}(r) \tag{3.26}$$

Defining $V_{eff}(r)$ as:

$$V_{eff}(r) = V_{ext}(r) + V_H(r) + V_{ext}(r) \tag{3.27}$$

where V_{ext} ,represents the external potential of the nuclei, V_H, the Hartree and V_{xc} the exchange correlation potential.

And

$$n(r) = \frac{2\Omega_c}{2\prod^3} \sum_j \int |\varphi_{kj}(r)|^2 \Theta(E_f - \varepsilon_{kj}) d^3k \tag{3.28}$$

Then spins up and down i.e. ↑ and ↓ are taken care of by the factor 2 and Θ is a step function which is either 1 or 0. E_f is the highest energy level occupied by single particle which is defined by the number of electrons *Ne* in the unit cell. This energy is termed as Fermi energy

$$\int n(r)\, d^3r \tag{3.29}$$

Electronic wave functions are expanded into k-points that are described in form of discrete set of plane waves; this is done according to Bloch's theorem. This theorem merges the number of electronic states at infinite problem to finite of calculating finite number of electronic states at an infinite number of **k**-points extended over a single unit cell. Although, this could be a minor improvement since there is need for an infinite number of calculations for the different **k**-points. But the electronic states at *k*-points close to each other are similar and therefore a possibility of representing the wave functions of a specific point of k-space by the wavefunction at a single **k**-point.

3.5.2 Reciprocal Space (Brillion Zone) and k-Points

In materials research, DFT is used for calculations in a system with periodic atoms in space. The cell, containing these atoms, which is repeated periodically, is called the supercell. These supercells are identified with the lattice vectors a_1,a_2, and a_3. To solve Schrödinger equations for a periodic system, the solutions must be in line with Bloch's theorem in which the solutions are written as:

$$\varphi_k(r) = e^{(ikr)}\mu_k(r) \tag{3.30}$$

where *k* is a wave vector associated to the Brillion first zone, *r* represents the position vector that defines a point in space, and $\mu_k(r) = \mu_k(r + n_1\alpha_1 + n_2\alpha_2 + n_3\alpha_3)$ for the integers n_1, n_2 and n_3 and are periodic functions and the space is periodic with a super cell of same periodicity. Bloch's theorem indicates that the Schrödinger equation can be solved independently for any value of *k*. The mathematical problems involved in DFT are simpler to solve with respect to *k* than *r*, (Sholl & David, 2009). Because the expansion of e^{ikr}express the original plane waves and calculations related in this equation are defined as plane-wave calculations. Plane waves allow for taking advantage of the fast Fourier transformation (FFT), hence it is the most numerically convenient basis set that can be used in DFT. The vector *r* represents the real space, and vector *k* is the reciprocal space (or k space), **(**Sholl & David, 2009).In *k* space, a unit cell has minimum volume containing all information of the material. The concept of the primitive cell in *k* space follows the Wigner-Seitz cell, in which the reciprocal lattice vectors are easily defined just like in real space. Cells in *k* space are often referred to as the Brillion zone, which contains several *k*-points with special significance of symmetry. These points are given independent identities. Gamma point (Γ point) is the most important point, which is the center of the reciprocal space

(i.e., k= 0 at the Γ point), (Sholl & David, 2009).The convergence of k-point mesh (n_i× n_i × n_i), where n_i=1, 2, 3 with respect to total energies (for the cubic structure of the BaF_2) is shown in the figure 3.2.

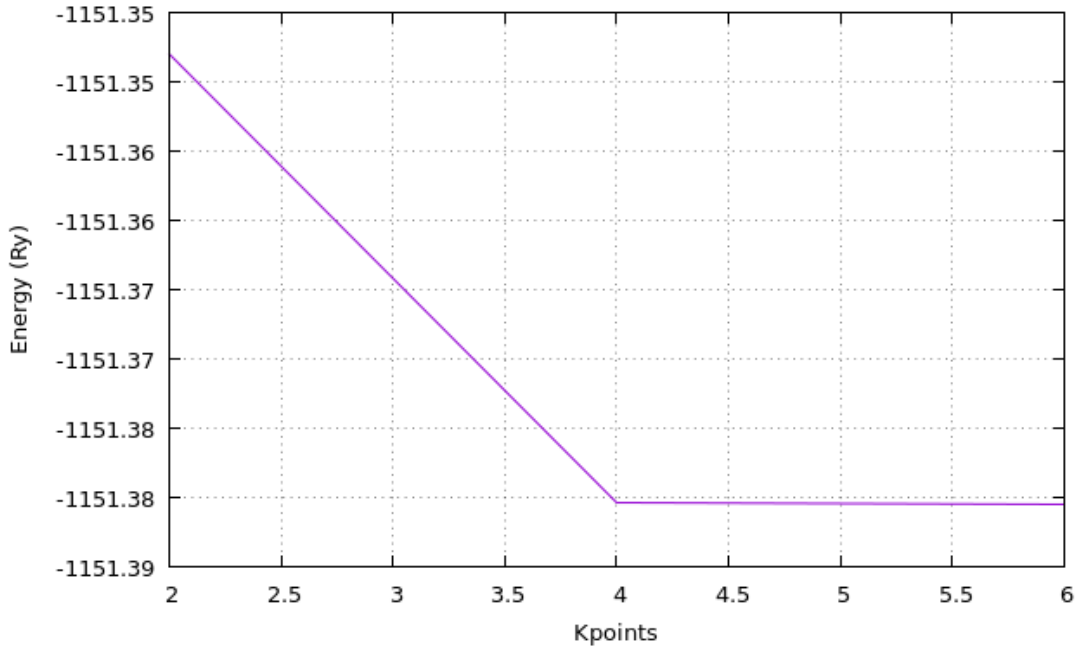

Figure 3.2: Convergence graph for K-points

DFT calculations require significant computational effort; therefore, integration of the mathematical equations cannot take place over the entire *k* space. Monkhorst and Pack, (Monkhorst & Pack, 1976) developed a solution, wherein a grid of points in *k* space is considered. For a super cell that has the same length in all directions (e.g., a cubic lattice), similar number of *k*-points are used in various directions. Calculation is then labeled as M×M×M k- points. Generally, it is expected that using M will give more accurate results than N, if M>N. However, practically, to decide how many *k*-points will be used depends on the material system. If the calculated total energy is almost independent of the number of **k-** points, then it is expected that all calculations

in **k** space are optimized well, and thus there is no need to use a large set of *k*-points, (Monkhorst & Pack, 1976).

3.5.3: Pseudo-Potential

The atomic potential $V(r)$describes the electrostatic interaction of the nucleus with the surrounding electrons. While each atom contains core electrons and valence electrons, the valence electrons are the ones responsible for the chemical bonding in atoms. The pseudo-potential method is developed capable to handle the valence electrons only. This approach is to cut computational cost in calculations (Mattsson, 2011). In this method, the "fixed" core electrons are eliminated. Inside the core region, the valence electron wave function is due to orthogonality to the core electron wave function described by a smooth node-less wave function while this is matched with the true wave function outside the core region (Smallwood *et al.*, 2006). A calculation without the frozen core is called an all-electron calculation. An illustration of matching wave functions in a pseudo-potential approach is shown in Figure 3.3.

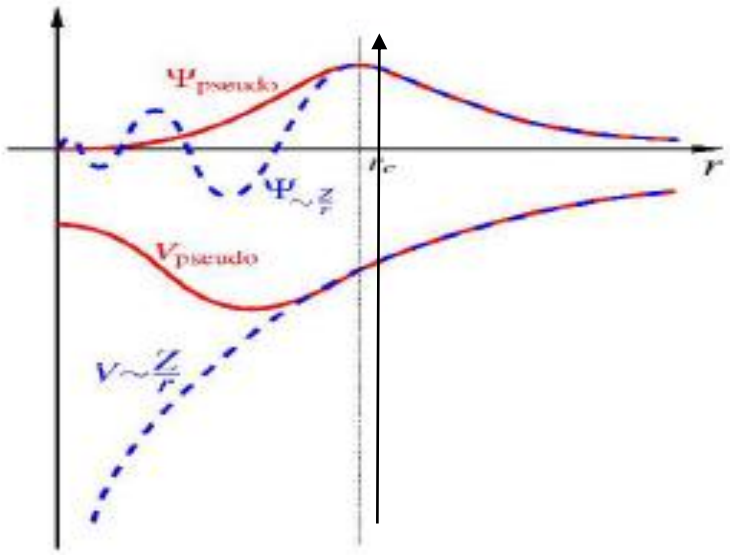

Figure 3.3: Pseudopotential of an atomic electron wave function.

The arrows indicate the cutoff radius of the wave functions, where the left of the arrow is fixed as the “frozen core” and the wave function is replaced by a smooth node-less function. To the right of the arrow, the pseudo-wave function matches the all electron wave function. The same behavior is shown, where the cutoff radius is set at a different value. This indicates that each valence state is set with a specific cutoff radius in the pseudo-potential approach. The pseudo-potential approach has increased the performance of DFT because the smooth functions can be expanded easily in plane wave calculations, (Sholl & David, 2009). Moreover, the use of pseudo-potential has cut down the computational costs since it eliminates the interactions from the core electrons.

3.5.4 Cut-Off Energy

In DFT methods, the energy associated with plane wave basis is very vital for the calculations that are involved. The optimization of cut-off energy in accordance to the total energy is examined at a constant *k*-point-mesh and experimental lattice parameters are achieved from the already obtained crystallographic databases. The cut-off optimized energy curve(for the structure of LaF_3) is shown in the Figure 3.4.

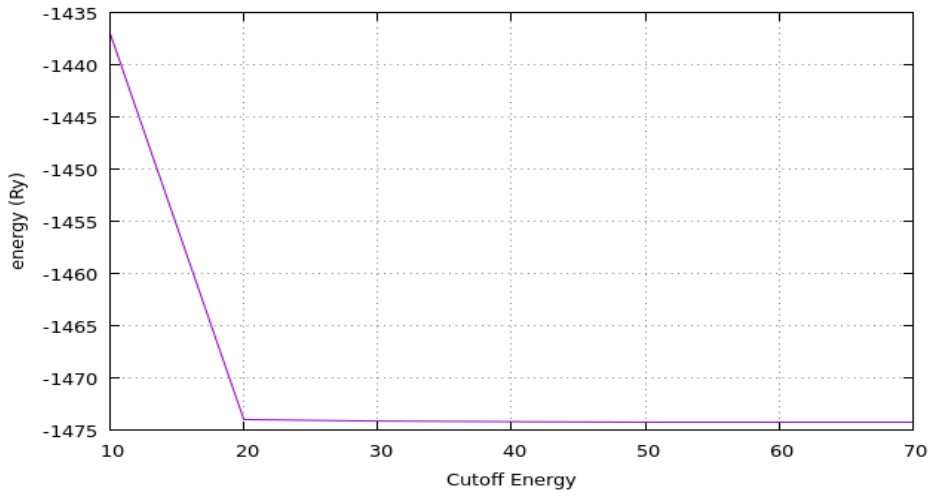

Figure 3.4: Cut-off optimized energy curve of LaF_3

It is advised that the values chosen may be above the default cut-off energy (30Ry) which may give accurate results. Energies picked from very high energy may not be advisable because they are associated to hiking the computational costs not considering if the results are accurate.

3.6 Structural Properties of Materials

Different materials have different structures that can be categorized by the magnitude of several features in general. Majorly, these features are grouped as follows: in the atomic structure, this includes features that are invisible, which include feature like the types of bonding between the atoms and the arrangement of atoms (Lundstrom,2002). Micro structure includes features that are visible by use of external devices for instance the microscope. These atomic structures ideally affect the optical properties chemical, thermal, electrical, magnetic, and the physical aspects of a material. Although macrostructure and microstructure are likely to affect these properties, they however affect elastic properties adversely and the chemical reaction rates of the material involved. Material properties open up the structure of the material This may be in line with the strength of metals, which in an engineering world that proposes that atoms are bounded by strong bonds and hence strong hints on the high chances of material applications in the real world (Manjula *et al.,* 2016). The arrangement of atoms and the type of atoms in a material are vital for the understanding of the structure of a material.

From microscopic point of view, the structural properties are vital in the understating of solids properties. We have done computation of the lattice parameters for tysonite LaF_3 structure. Total energy of LaF_3 was obtained in terms of volume unit-cell around

the equilibrium cell volume ($V_{0,}$) and then the E-V points obtained were fitted into the equation of state (EOS) to obtain derived structural properties. The Birch-Murnaghan third-order (Murnaghan, 2017) equation of state written as:

$$\Delta E(V) = E - E_o = B_0 V_0 + \left[\frac{V_0}{B_0} + \frac{1}{1 - B_0^{'}} + \frac{V_0^{'-B_0}}{B_0^{'}\left(B_0^{'} - 1\right)} \right] \quad (3.31)$$

where E_0 is the equilibrium energy, (B_o) is the bulk modulus; ($B_o^{'}$) is the first derivative of materials, when the constants differ; Strains tend to be introduced into the layer ones the parameters are different leading to hindrance of epitaxial growth of thicker layers without defects (Ravindran *et al.,* 1998).

3.7 Electronic Properties

Electronic structure of a material can be related to the movement of electrons in an electrostatic field generated by nuclei that are stationary (Diebold, 2003). Electronic properties describe the wave functions of the electrons and the energies involved. By solving quantum mechanical equations, electronic structural properties of a material are achieved; the band structure and density of states among others that can describe electronic properties vividly.

3.7.1 Band structure and Band gaps

The range of energy that electrons can posses inside a solid can be used to give a band structure description of a solid. This energy is associated to energy bands, allowed bands, or forbidden bands which are basically ranges of energy which may not be also termed as band gaps (Scandolo *et al.,* 2005). Band gaps can be related to these ranges of energy that are free from any band that makes up energy bands of finite widths. The bands have different widths. The width of different bands depends on the overlap degree of atomic orbitals from their arrangement. The range of energy may not be

covered fully by any two adjacent bands due to their width. For instance, 1s electrons related to the core orbitals are narrower as a result of small overlap with the atoms surrounding them. This phenomenon has led to increase in band gaps between the core bands. Bands at higher levels includes bigger and bigger orbitals with most overlap, becoming wider and wider in increasing steps at high energy until there are no band gaps at high energy depending on the degree of overlap in the atomic orbitals from which they arise. Band gaps are categorized either as direct band gaps or indirect band gaps. Particular crystal momentum (k-vector) in the Brillion zone distinguishes between energy state at minimum in the conduction band and the energy state in the valence band maximum. For similar k-vectors then this becomes a direct band gap. The momentum of electrons and holes are similar in both the conduction band and the valence band that is an electron can emit a photon directly. Any differences in k-vector then an indirect band gap is formed and this means that a photon cannot be emitted and therefore an electron must pass through an intermediate state and transfer momentum to the crystal lattice (Granqvist & Hulta, 2002). Direct and indirect band gaps are illustrated in figures 3.5 and 3.6

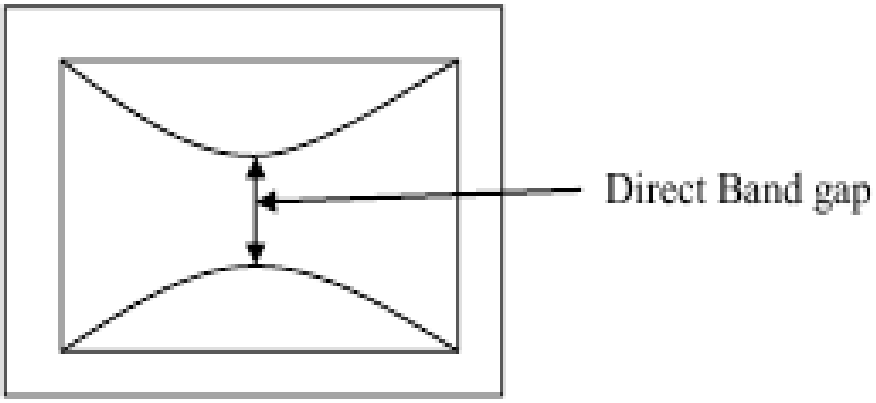

Figure 3. 5: Illustration of a direct band gap in a material

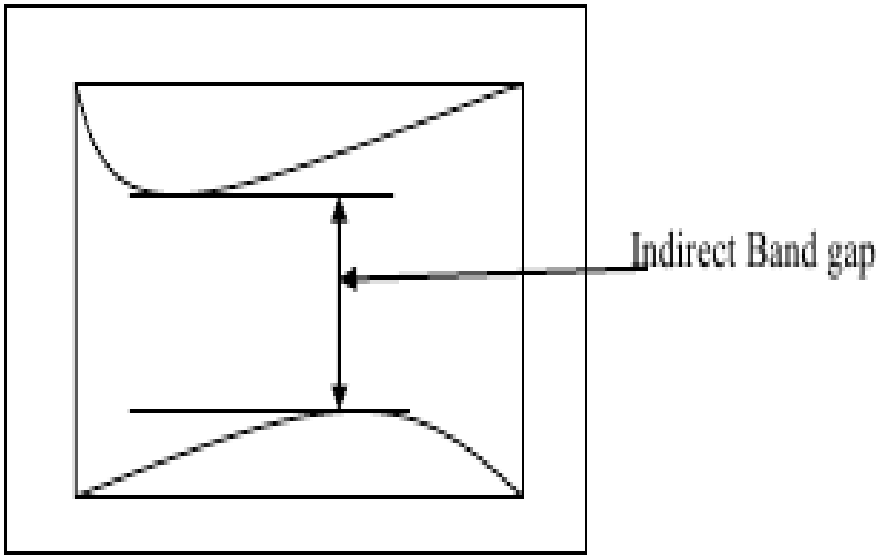

Figure 3. 6: Illustration of an indirect band gap in a material

3.7.2 Density of states (DOS)

Density of states of materials can be best defined as the number of states divided by the energy interval for every single energy level that electrons available can occupy. Apart from special cases such as the atoms or molecules in gas phase systems, the

density distributions are continuous not discrete like a spectral density. A high density of states at a specific energy level means that the states available for occupation are many. Zero density of states refers to no states that can be occupied at any energy level. Generally density of states is an average of space occupied by the system over time domains.

3.7.3 Electronic Properties of BaF_2 and BaF_2: La

A supercell corresponding to 2 x2 x 2 conventional unit cells using phonopy code (Atsushi & Isao, 2015) which translated into 24 atoms was built. The supercell was used for defect calculations to prevent the contribution of defect-defect interaction from the calculation of formation energy. One barium atom was substituted with a lanthanum atom and one fluorine atom was placed in an interstitial position in BaF_2 supercell for charge compensation. The influence of La as well as the interstitial fluorine on the BaF_2 band structure and the elastic constants were studied and compared with the data of BaF_2.Weigner-Seitz cell may be defined as a cluster of points that surrounds a specified point in a given region that are nearer the lattice point than to any other points. The Brillion Zone (BZ) gives a thorough geometrical definition of diffraction conditions such as the electron energy band theory.

A supercell has an advantage that the electronic structure of the host crystal is the same. That is, the calculations for a supercell which is simply filled with the host crystal without a defect reproduces the same electronic structure properties like band structure of a single crystal. Electronic band structure of BaF_2:La has also been investigated at the high symmetry points of the barium fluoride in its cubic phase within the Brillion zone. The band structure characteristics of tysonite LaF_3 were also

studied. Band gap and Density of states (DOS) helps in the understanding of how superconductivity and superionic transitions occur in LaF_3 hence mechanism to improve conduction in all faculties of its application can be studied. For the band structure of LaF_3 for a tysonite phase the high symmetry points used were Γ-M-K-Γ-A-L-H-A/L-M/K-H. The X-window Crystalline and Molecular Structure Visualization (XCrysDen) program was used to come up with these points and path.

3.7.4 Elastic constants of LaF_3

Elastic constants majorly define mechanical and dynamical characteristics, especially the stability and the stiffness of a material. The inter-atomic forces have been probed by using these parameters (Sinko & Smirnow, 2002). Although LaF_3 belongs to tysonite structure, its mechanical properties were calculated within the hexagonal phase group of crystals, with six independent elastic constants. *Ab initio* calculations have bared a lot of fruits in obtaining elastic properties indifferent materials especially theoretically (Shrader *et al.*, 2014).For instance, elastic constants are generated from energy variation by application of a little strain to the converged lattice configuration. This energy in consideration can be written as:

$$\Delta E = \frac{V}{2}\sum_{i=1}^{6}\sum_{j=1}^{6} C_{ij} e_i e_j \quad (3.32)$$

V= volume of the original lattice cell, ΔE= energy increase from the strain with vector e= (e_1, e_2, e_3,e_4,e_5, e_6) and C =matrix of the elastic constant. For the hexagonal phase, its primitive vectors can be denoted as:

$$\begin{pmatrix} a_1 \\ a_2 \\ a_3 \end{pmatrix} = \begin{pmatrix} \frac{\sqrt{3}a}{2} & \frac{1a}{2} & 0 \\ \frac{-\sqrt{3}a}{2} & \frac{1a}{2} & 0 \\ 0 & 0 & c \end{pmatrix} \tag{3.33}$$

a and c are lattice constants

A strain defined as $e = (\delta, \delta, 0,0,0,0)$ was applied to obtain $C_{11} + C_{12}$:

$$\frac{\Delta E}{V} = (C_{11} + C_{12})\delta^2 \tag{3.34}$$

$C_{11} - C_{12}$ was obtained using $e = (0,0,0,0,0, \delta)$:

$$\frac{\Delta E}{V} = \frac{1}{4}(c_{11} - c_{12}) \tag{3.35}$$

C_{33} was then obtained using the strain$e = (0,0, \delta, 0,0,0)$:

$$\frac{\Delta E}{V} = \frac{1}{2} C_{33}\delta^2 \tag{3.36}$$

$e = (0,0,0, \delta, \delta, 0)$ was used to obtain C_{44}:

$$\frac{\Delta E}{V} = (C_{44})\delta^2 \tag{3.37}$$

Under the condition of hydrostatic pressure, $e = (\delta, \delta, \delta, 0,0,0)$, the bulk modulus was also calculated by the equation;

$$B = \frac{2}{9}\left(C_{11} + C_{12} + 2C_{13} + \frac{C_{33}}{2} \right) \tag{3.38}$$

$$\frac{\Delta E}{V} = \frac{9}{2} B\delta^2 \tag{3.39}$$

Hence C_{13} is determined.

Appropriate averaging procedures can be used to obtain isotropic elastic constants .For example the bulk, shear and Young modulus. The three commonly used averaging methods implemented in Thermo_pw code are the Voigt approach (Voigt, 1928), which assumes a uniform strain, while the Reuss procedure validates

the case of uniform stress (Reuss, 1929) .The combination of the two approaches results to Voigt and Reuss moduli which are represented as stiffness constant. The bulk and shear modulus in the Voigt approach:

$$B_V = \frac{1}{9}\left[C_{11} + C_{12} + C_{13} + 2\left(C_{12} + C_{13} + C_{23}\right)\right] \tag{3.40}$$

$$G_V = \frac{1}{15}\left[\left(C_{11} + C_{22} + C_{33}\right) - \left(C_{12} + C_{13} + C_{23}\right) + 3\left(C_{44} + C_{55} + C_{66}\right)\right] \tag{3.41}$$

According to the Voigt-Reuss-Hill (VRH) approximation (Hill, 1952) the shear and bulk moduli of the polycrystalline material were approximated as arithmetic mean of the Voigt and Reuss limits:

$$B_{VRH} = \frac{1}{2}\left(B_v + B_R\right) \tag{3.42}$$

$$G_{VRH} = \frac{1}{2}\left(G_v + G_R\right) \tag{3.43}$$

From bulk modulus and shear modulus the Young modulus and Poisson ratio are then obtained.

3.7.5 Elastic constants of BaF_2:La

The calculation of elastic constants for BaF_2:Lawas done in the cubic phase of the host cubic phase of BaF_2.The cubic phase comprises of C_{11}, C_{12} and C_{44} elastic constants. Unlike the hexagonal structure, cubic elastic constants are less tedious to calculate and vectors are written as;

$$\begin{pmatrix} a_1 \\ a_2 \\ a_3 \end{pmatrix} = \begin{pmatrix} 0 & \frac{a}{2} & \frac{a}{2} \\ \frac{a}{2} & 0 & \frac{a}{2} \\ \frac{a}{2} & \frac{a}{2} & 0 \end{pmatrix} \tag{3.44}$$

where a is the lattice parameter, when a strain is applied, the primitive vectors are changed to the new vector written as

$$\begin{pmatrix} a_1^{'} \\ a_2^{'} \\ a_3^{'} \end{pmatrix} = \begin{pmatrix} a_1 \\ a_2 \\ a_3 \end{pmatrix} \cdot (1+\varepsilon) \tag{3.45}$$

ϵ =strain tensor which is linked to e = strain vector :

$$\varepsilon = \begin{pmatrix} e_1 & \frac{e_6}{2} & \frac{e_5}{2} \\ \frac{e_6}{2} & e_2 & \frac{e_4}{2} \\ \frac{e_5}{2} & \frac{a}{2} & e_3 \end{pmatrix} \tag{3.46}$$

e = (0, 0, 0, δ, δ, δ) (strain) is applied to the crystal (Ravindran *et al.*, 2001). Then C_{44} can be calculated from the equation;

$$\frac{\Delta E}{V} = \frac{3}{2} C_{44} \delta^2 \tag{3.47}$$

Shear modulus $C'$is obtained from the volume-conserving strain e = (δ, δ, $(1 + \delta)^{-2}$ - 1,

0, 0, 0) using the relation;

$$\frac{\Delta E}{V} = 6C'\delta^2 + 0(\delta)^2 \tag{3.48}$$

$$C' = \frac{1}{2}(c_{11} - c_{12}) \quad (3.49)$$

Lastly, bulk modulus B can be calculated from the strain under hydrostatic pressure e = (δ, δ, δ, 0, 0, 0), (Wang & Ye, 2003)

$$\frac{\Delta E}{V} = \frac{9}{2} B\delta^2 \quad (3.50)$$

By substituting the values appropriately, the three elastic constants can be determined from these relations and this was done using the thermo_pw code and the results were compared to those of BaF_2.

3.8 Defect Formation Energy

The defect formation energies of isolated La impurities in BaF_2 were studied. The single defects are interstitial for fluorine atoms and La substitution impurities. The complex defects are formed by a F interstitial in association with one La atom. A 24 atom supercell was built in study of defect properties .The cell contained 8 barium atoms and 16 fluorine atoms.

3.8.1 Interstitial formation energy

For interstitial formation energy calculations, the total energy of the relaxed perfect crystal (E_{perf}) was first calculated before introducing an interstitial. After introducing La atom together with an interstitial fluorine into the relaxed system, the crystal was again relaxed to achieve the optimized total energy of the system with an interstitial, E_{La}. The calculations were carried out at ground state conditions. Interstitial formation energy equation was used to calculate the formation energy (Kuznetsov *et al.*, 2003);

$$E_{def} = E_{La} + E_{perf} - E_F^{at} - E_{La}^{at} + E_{Ba}^{at} \quad (3.51)$$

where E_F^{at}, E_{La}^{at} and E_{Ba}^{at} are the energies for single atoms for fluorine, lanthanum and barium respectively.

The energy difference between the bulk super-cell and the relaxed super-cell containing the lanthanum defect determined the defect formation energy of the interstitial

3.8.2 Neutral charge formation energy

The neutral charge formation energy was also carried out by including a neutral charge in the calculation which hindered the inclusion of interstitial charge compensation fluorine and this translated to 24 atoms instead of 25 atoms. The defect formation energy was then obtained from the energy difference between the defected super-cell with lanthanum substitute and the relaxed pure super-cell without a defect. These results were compared to the interstitial formation energy to get the most stable system.

3.9 Optical properties

The materials constants like the dielectric constant ε_1, the conductivity σ_1, and the permeability μ_1 represent the charge of the field and the current present in matter. Because of simple historical reasons, refractive index *n* and the extinction coefficient *k* optical constants have been associated extensively with the propagation and dissipation of electromagnetic waves in different media. Description of optical properties in different media requires the definition of complex refractive index as a new response function written in the form.

$$\widehat{N} = n + ik = \left[\varepsilon_1\mu_1 + i\frac{4\pi\varepsilon_1\sigma_1}{\omega}\right]^{\frac{1}{2}} = [\widehat{\varepsilon}\,\mu_1]^{\frac{1}{2}} \tag{3.52}$$

where the complex wavevector value q=$q\hat{}n_q$ and n_q = **q**/q is the unit vector along the q direction and is written

$$\hat{q} = \frac{\omega}{c}\hat{N} = \frac{n\omega}{c} + i\frac{k\omega}{c} \tag{3.53}$$

The refractive index *n* and the extinction coefficient *k* can be written in terms of conductivity σ_1, the permeability μ_1, and the dielectric constantε_1 (Gajdoš *et al.,* 2006)

$$\hat{n}^2 = \frac{\mu_1}{2}\left\{\left[\varepsilon_1^2 + \left(\frac{4\pi\sigma_1}{\omega}\right)^2\right]^{\frac{1}{2}} + \varepsilon_1\right\} \tag{3.54}$$

$$\hat{k}^2 = \frac{\mu_1}{2}\left\{\left[\varepsilon_1^2 + \left(\frac{4\pi\sigma_1}{\omega}\right)^2\right]^{\frac{1}{2}} - \varepsilon_1\right\} \tag{3.55}$$

Equations (3.54) and (3.55) give two vital relations that contain important relation of the electromagnetic wave propagation in materials. The optical constants describe wave propagation and are incapable of describing direct current properties of materials. For ω=0, ε_1, $\sigma_1$and μ_1 are the only constants defined. The reflectivity of a dielectric material without losses k-0 the refractive and extinction coefficient *k* becomes:

$$n^2 - k^2 = \varepsilon_1\mu_1 \tag{3.56}$$

$$2nk = \frac{4\pi\mu_1\sigma_1}{\omega} \tag{3.57}$$

Equation (3.57) can be written as in terms of dielectric constant, permeability and the conductivity;

$$\widehat{N^2} = \mu_1\left[\varepsilon_1 + i\frac{4\pi\sigma_1}{\omega}\right] = \mu_1\hat{\varepsilon} \approx \frac{4\pi i\mu_1\sigma_1}{\omega} \tag{3.58}$$

If $|\varepsilon_1| \geq 1$ then

$$\left|\widehat{N}\right| = (n^2 + k^2)^{\frac{1}{2}} \tag{3.59}$$

3.9.1 Reflectivity

The reflectivity R(ω) can be expressed as

$$R(\omega) = \left[\frac{1-\widehat{N}}{1+\widehat{N}}\right]^2 = \frac{(1-n)^2+k^2}{(1+n)^2+k^2} \tag{3.60}$$

If $k \to 0$then the reflectivity is reduced to:

$$R = \left|\frac{1-n}{1+n}\right|^2 \tag{3.61}$$

The complex imaginary dielectric function $\varepsilon_1(\omega)$ has been obtained by summing over conduction bands (Ambrosch & Sofo 2006):

$$\varepsilon_{\alpha\beta}^{(2)}(\omega) = \frac{4\pi^2 e^2}{\Omega}\frac{1}{q^2}\lim_{q\to 0}\sum_{c,v,k} 2w_k \delta(\epsilon_{ck} - \epsilon_{vk} - \omega) \times \langle u_{ck+eaq}|u_{vk}\rangle \langle u_{ck+eaq}|u_{vk}\rangle^*$$

(3.62)

Equation (3.62) indicates a transition between the occupied and the unoccupied states within the first Brillion zone and the *k* vectors wave are fixed. The Kramers-Kronig relation connects between the real and the imaginary parts of an analytical dielectric function (Harrison,1999) as;

$$\varepsilon_{\alpha\beta}^{(1)} = 1 + \frac{2}{\Pi} P \int_0^\infty \frac{\varepsilon_{\alpha\beta}^{(2)}(\omega')\omega'}{\omega^{2\prime}-\omega^2+i\eta} d\omega' \tag{3.63}$$

The complex dielectric constant ε̂ and the complex conductivity σ̂ can be regarded as the prime response functions to the applied electric field.

3.9.2 Absorption coefficient

The absorption coefficient corresponds to the intensity loss per unit length ($I(x) = I_o \exp(-ax)$) which is given as:

$$\alpha(\omega) = \frac{\omega}{4\pi}\varepsilon_2(\omega) \tag{3.64}$$

It can be indicated from the equation that there is a strong relationship between α (ω) and ε_2 (ω) although an exact ω dependence will cause an increase in high-energy absorption. The frequency dependent dielectric matrix was calculated using quantum espresso optical programs. Imaginary dielectric and real dielectric values of BaF_2:La were obtained. The reflection, refractive indexes were then calculated using real and imaginary parts of dielectric function.

CHAPTER FOUR

RESULTS AND DISCUSSIONS

4.1 Results

The tysonite phase structure is presented in figure 4.1. In a DFT calculation, computations were done at 0 K in which our calculations have been carried out.

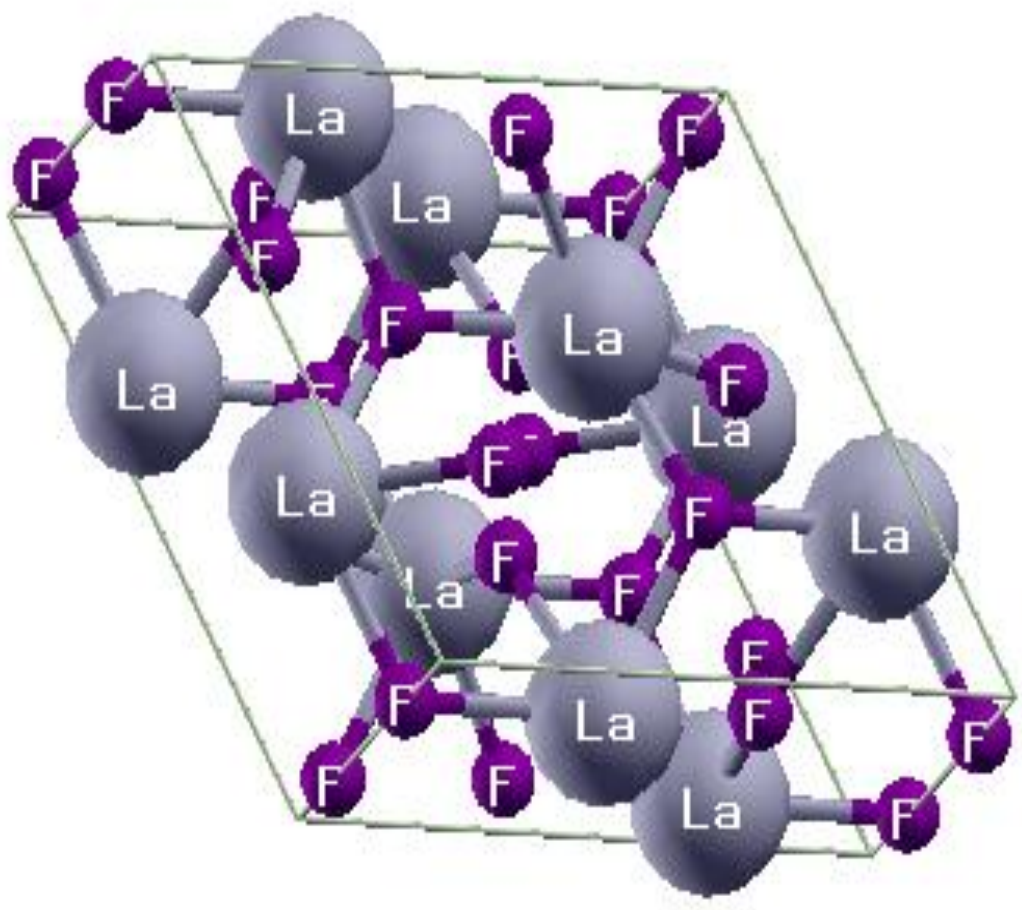

Figure 4. 1: The LaF_3 tysonite structure

The tysonite structure of LaF_3 belongs to the space group *P-3c1* (No. 165). There are six formula in the unit cell and the initial atomic Wychoff positions are La (0.6597, 0,

1/4), F 1 (0.3656,0.0535, 0.0813), F 2 (1/3, 2/3, 0.1865) and F 3 (0, 0, 1/4) respectively (Belzner *et al.*,1994)

Table 4. 1: Lattice constants, volume per atom and bulk modulus for LaF_3

	a (Å)	c(Å)	c/a	V_0(Å^3)	B_0(GPa)	B'$_0$	REFERENCES
PRESENT WORK	7.245	7.388	1.02	327.14	114.44	4.25	(Elicah *et al.*,2018)
CASTEP(LDA)	7.128	7.329	1.028	322.48	114.26	3.96	(Zhenlong *et al.*,2014)
WIEN2K(GGA)	7.260	7.427	1.023	339.01	97.27	-	(Modak *et al.*,2009)
EXPT	7.191	7.357	1.023	329.46	104.9	4.5(6)	(Crichton *et al.*,2010)

From the results presented ,a statistical-correlation exists between the calculated and experimentally obtained values; this is evident from smallest deviations seen in lattice parameters. The results obtained in this study compare favorably well with other calculated values. From table 4.1, it can be deduced that the deviations in optimized lattice parameter values are less than 1 % from the experimental values obtained.

4.1.1 Phase Stability of LaF_3

LaF_3 exists in three phases namely: tysonite, orthorhombic and tetragonal. The phase stabilities of these phases of LaF_3 were obtained; the total energies were calculated at fixed volumes followed by energy-volume relationships analysis. The energy against volume for these phases of LaF_3 were as illustrated in figure 4.2. The tysonite phase structure had the minimum energy and therefore it was the most stable at ground state compared to the orthorhombic and tetragonal phases.

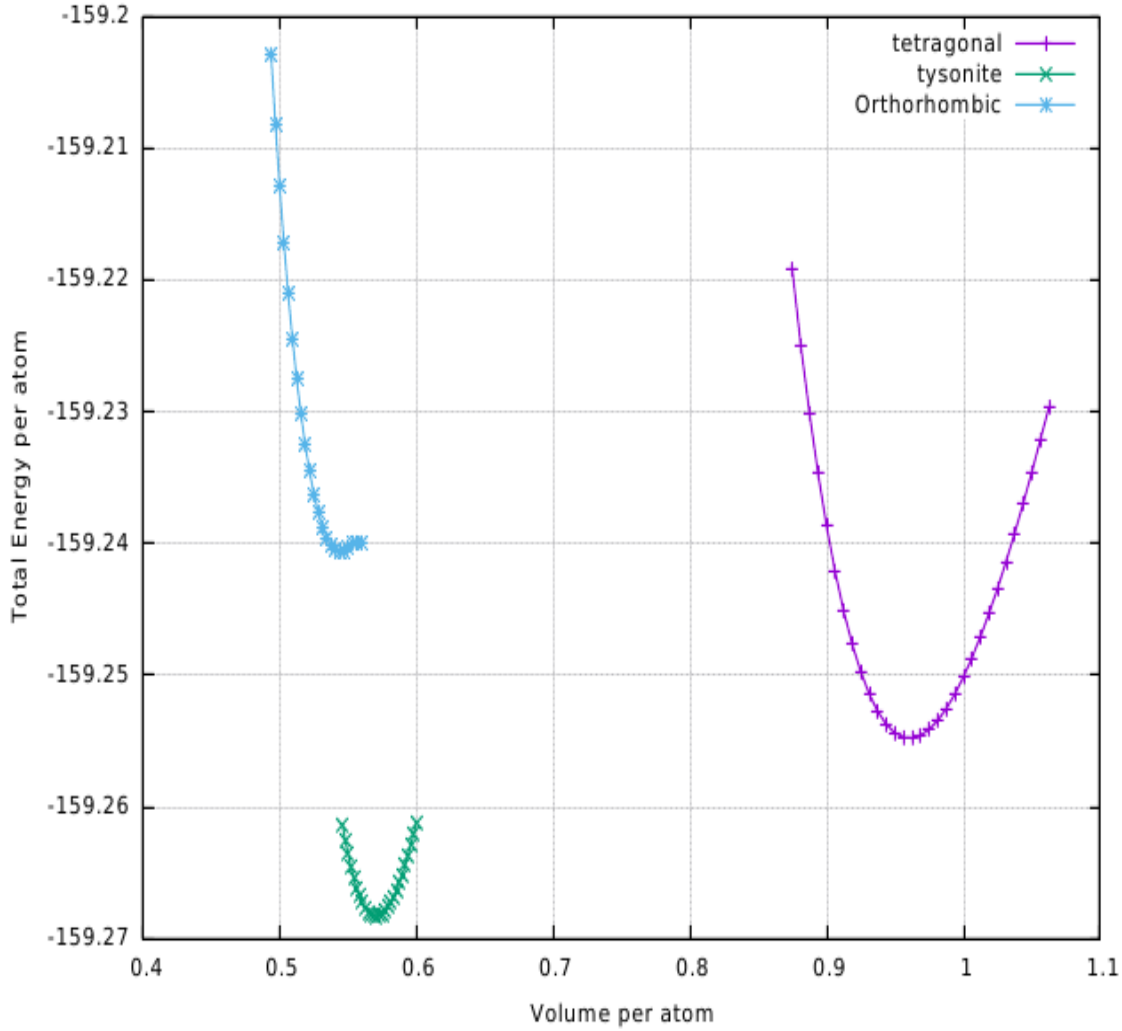

Figure 4. 2: Phase stability for LaF_3 phases

4.1.2 Structural properties of BaF_2 and BaF_2: La

A supercell of 2*2*2 was constructed from a unit cell of BaF_2 which translated into 24 atoms. Barium atom was then substituted with La. But since Lanthanum has an extra electron, a charge compensation was done by incorporating interstitial fluorine.

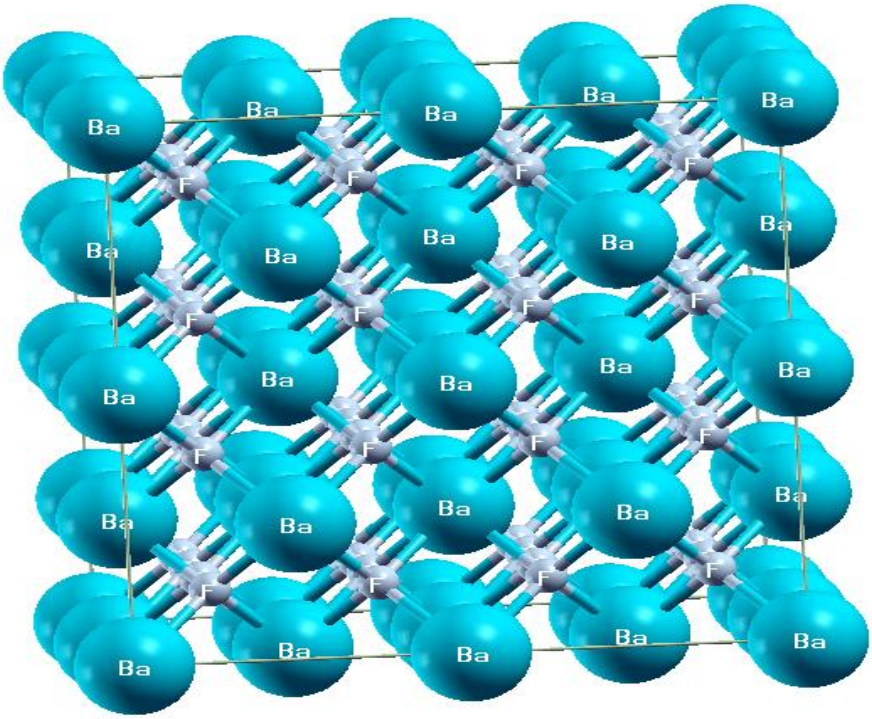

Figure 4. 3: A supercell of BaF_2

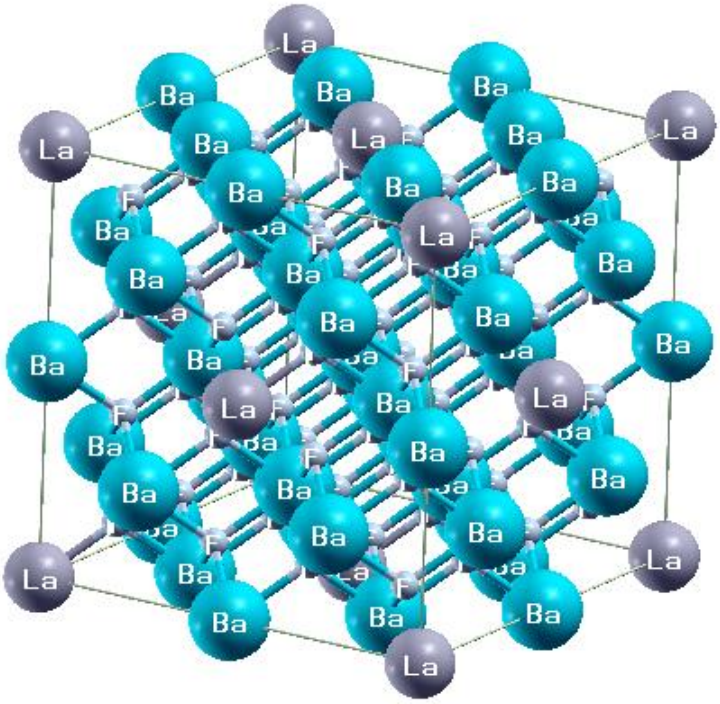

Figure 4. 4:Supercell structure of BaF_2: La

4.1.3 Electronic properties of LaF_3

The band structure and the density of states (DOS) play an important role in analyzing the electronic properties of materials. The band structure of LaF_3 is shown in figure 4.5

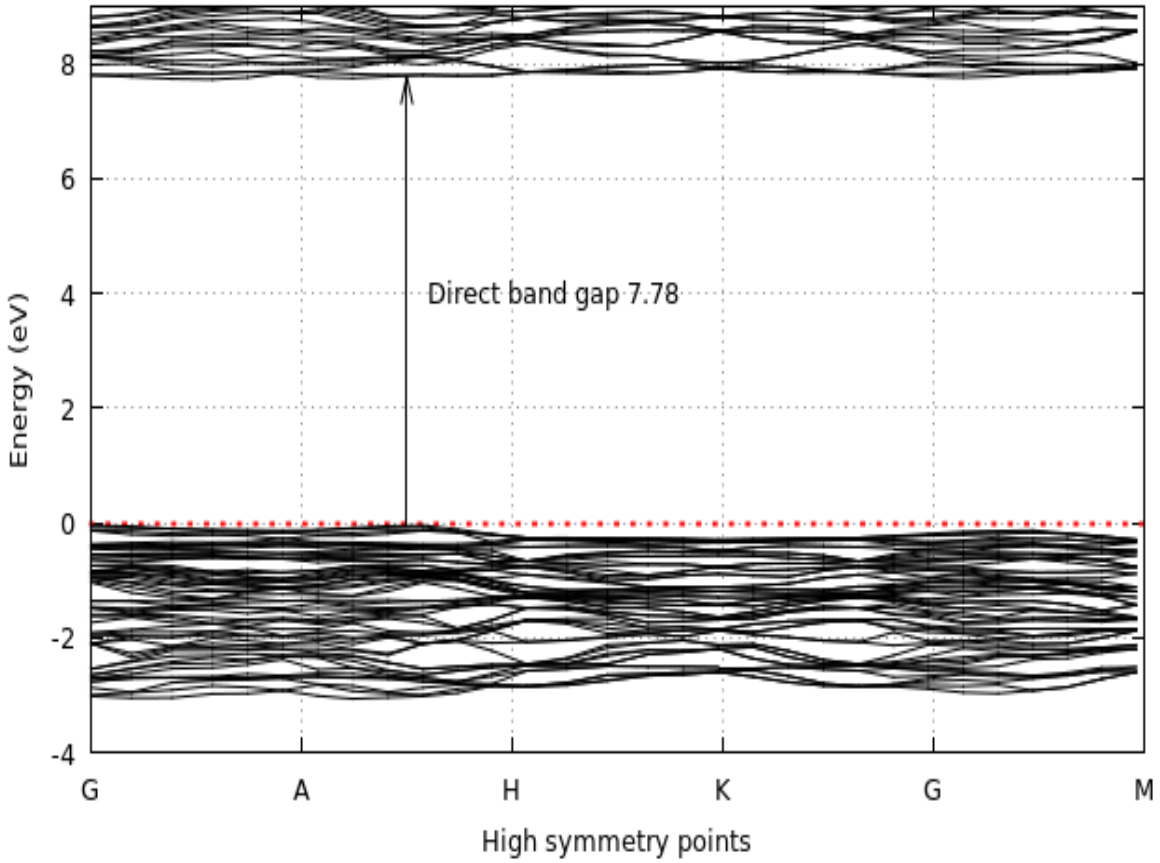

Figure 4. 5: LaF_3 band structure

From the calculations it is shown that LaF_3 is a wide-band-gap insulator with a direct band gap of 7.78 eV. Compared with the value of 6 eV calculated by Modak (Modak *et al.*, 2009) through Wein2K code, these results are closer to the experimental data of 9.7 eV. It is well known that the DFT usually underestimates the band gap, thus

these value should be reasonable. It is well known that the DFT usually underestimates the band gap, this is because of the existence of a derivative discontinuity of energy with respect to number of electrons (Perdew *et al.*,1996).

The density of states for LaF_3 are as illustrated in figure 4.6

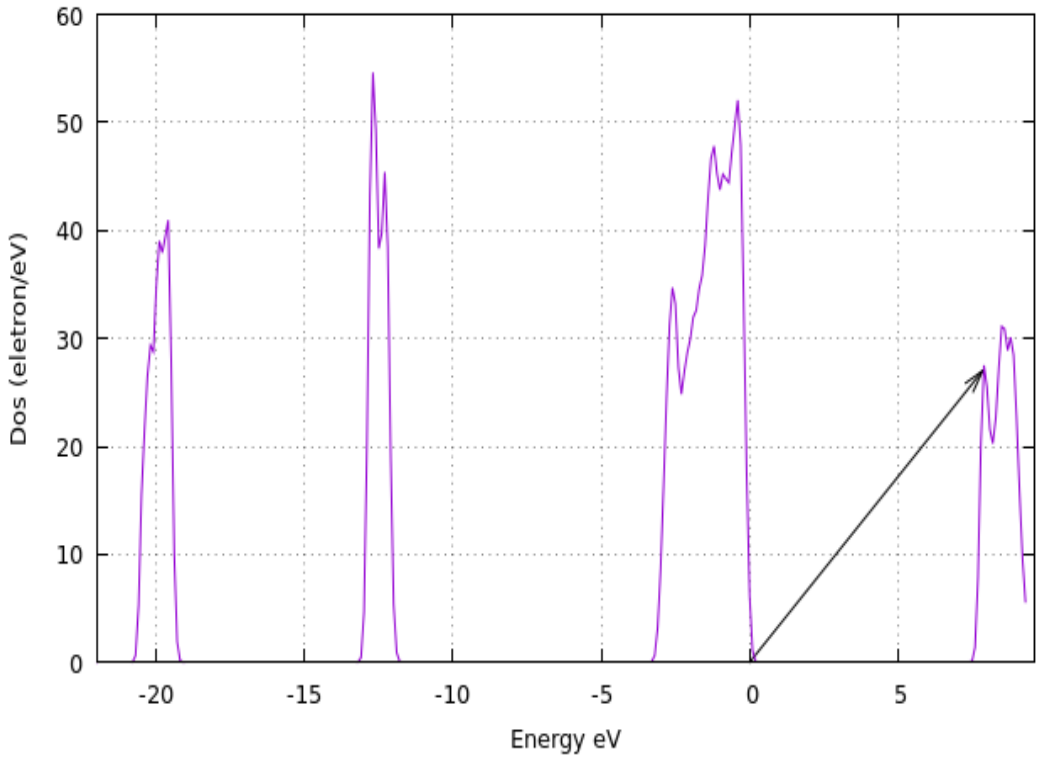

Figure 4. 6: Density of states of LaF_3

The density of states illustrates that the conduction band is majorly occupied by the La-5p states and the La-5d states. The valence band is dominated by F-2p state majorly.

Table 4*. 2*: Band gap values for tysonite LaF_3

Direct band gap (eV)	CASTEP (LDA) 7.76	WEIN2K 6.0	EXPT 9.7	GGA 7.78
Ref	(Zhenlong *et.al.*,2014)	(Modak *et.al.*,2009)	(Belzner *et.al.*,1999)	(Elicah *et al.*,2018)

The band structure and the density of states obtained are as presented in Figure 4.5 and Figure 4.6 respectively. The gap above the highest occupied energy level and the lowest unoccupied energy level is equivalent to the difference in the valence band maximum and conduction band minimum. The band structure indicates that the tysonite phase of LaF_3 is a strong insulator having a direct band gap of 7.78eVwhich is comparable to experimental value of 9.0 eV. The band gap values are tabulated in Table 4.2 for further comparisons. The results obtained can be compared well with other theoretical results. The band gap obtained in this work is underestimated as compared to the experiment value as expected from the pseudopotentials used.

4.1.4 Electronic properties of BaF_2 and BaF_2:La

The band structure, band gap and density of states of BaF_2 are presented in Figures 4.7 and 4.8 respectively.

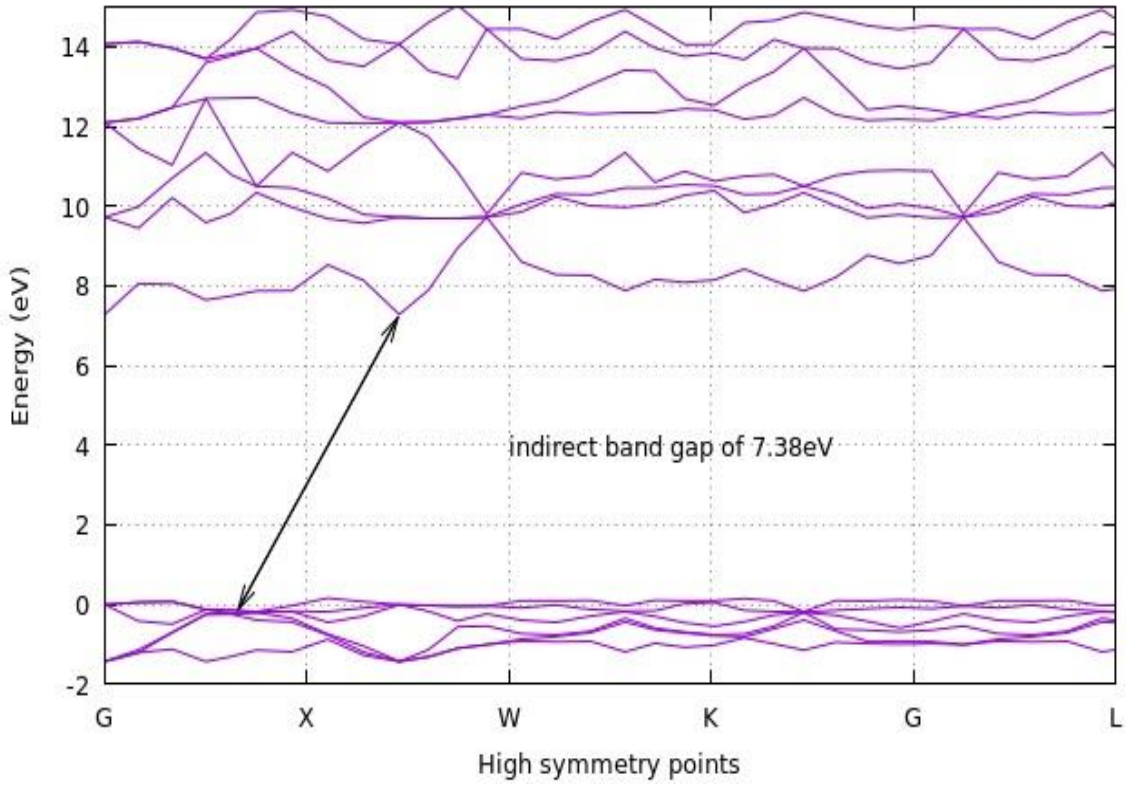

Figure 4.*7*: Band structure of BaF_2

The valence and conduction band structure of the cubic BaF_2 is displayed in figure 4.7 where an ionic and cationic states are expected to constitute the top of the valence band and the bottom of the conduction band respectively. Accordingly, the F 2p states form the upper valence band followed by a band due to the Ba 5p states at about 7.38 eV below the top of the valence band.The results yielded location of the outermost core band (due to the Ba 5p states) in excellent agreement with the reflection and photoelectron experiments which report the band gap to be at about 7.8 eV below the valence band (Itoh & Itoh,1992). It is to be noted here that calculations based on DFT provide a very good description of electronic states in the valence band, though they are not as reliable in describing the conduction states.

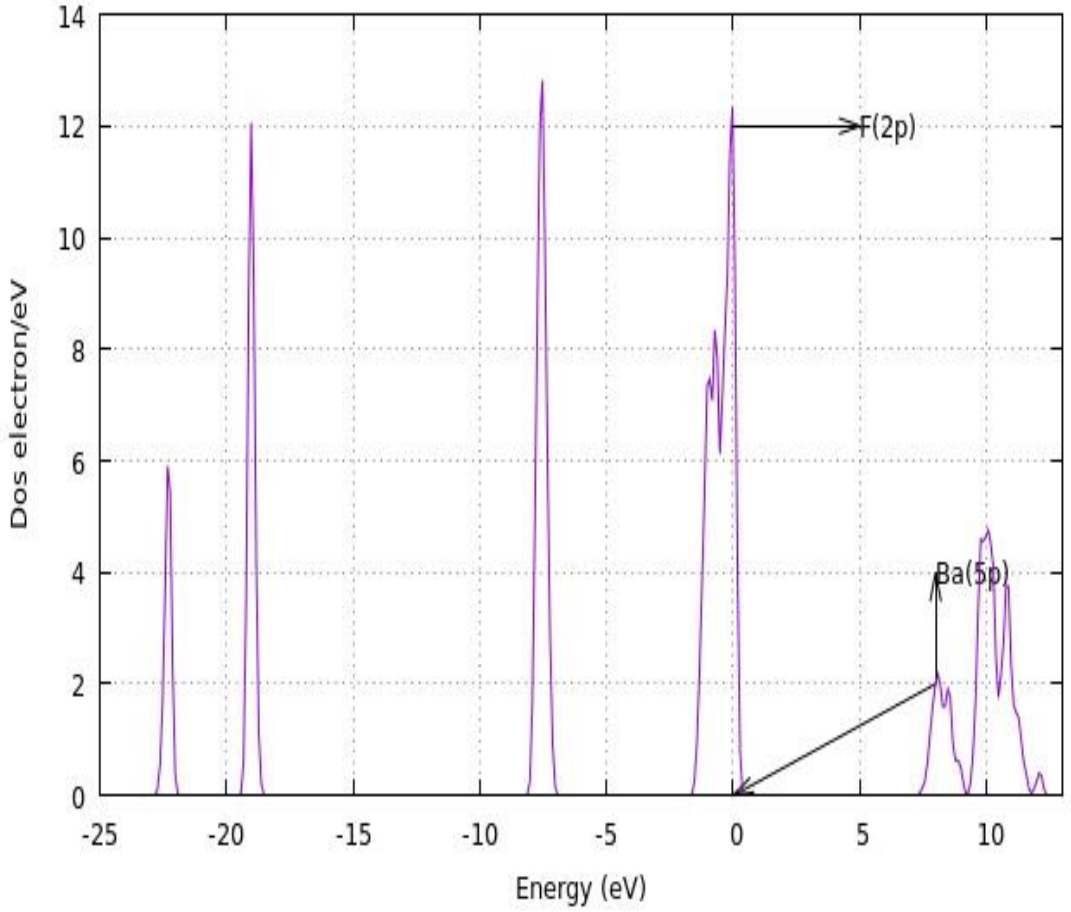

Figure 4. 8: Density of states of BaF_2

The calculated density of states (DOS) of the cubic BaF_2 using the GGA method is as presented in Figure 4.8.From the figure it is shown that the upper valence bands (VB) mainly consist of F *p*-spin, whereas the conduction band (CB) bottom consists essentially of Ba *p*-spin. The orbital contribution from F atoms is small in this energy range. This results fits to the previous theoretical study obtained earlier (Catti *et al.*,1991).

Band structure and density of states for BaF_2:Laare as shown in figures 4.9 and 4.10.

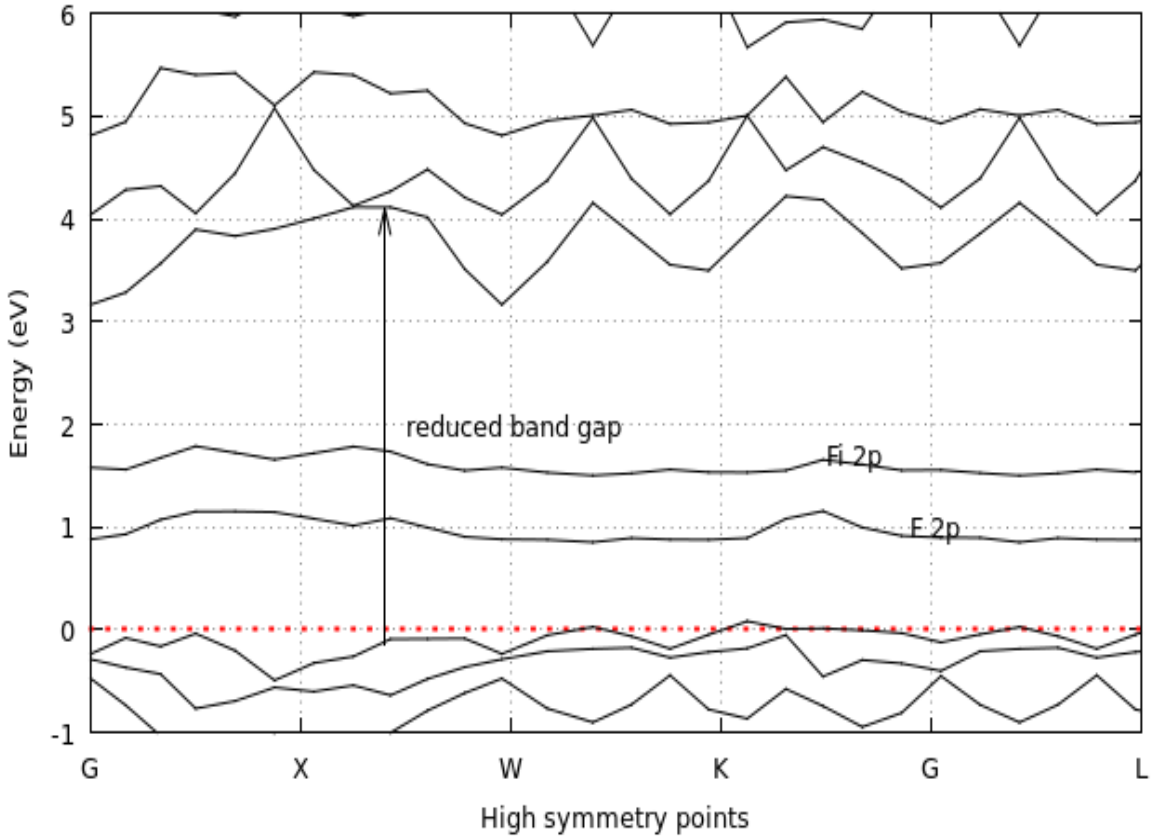

Figure 4. 9:Band structure of BaF_2: La

The valence band of BaF_2 is constituted by states of both Ba and F, while the cation states dominate conduction band respectively. The main effect of introduction of the La^{3+} results into the appearance of the upper electronic band connected to the interstitial F_i 2p.The broadened valence band is as a result of the introduction of La-5p in BaF_2.

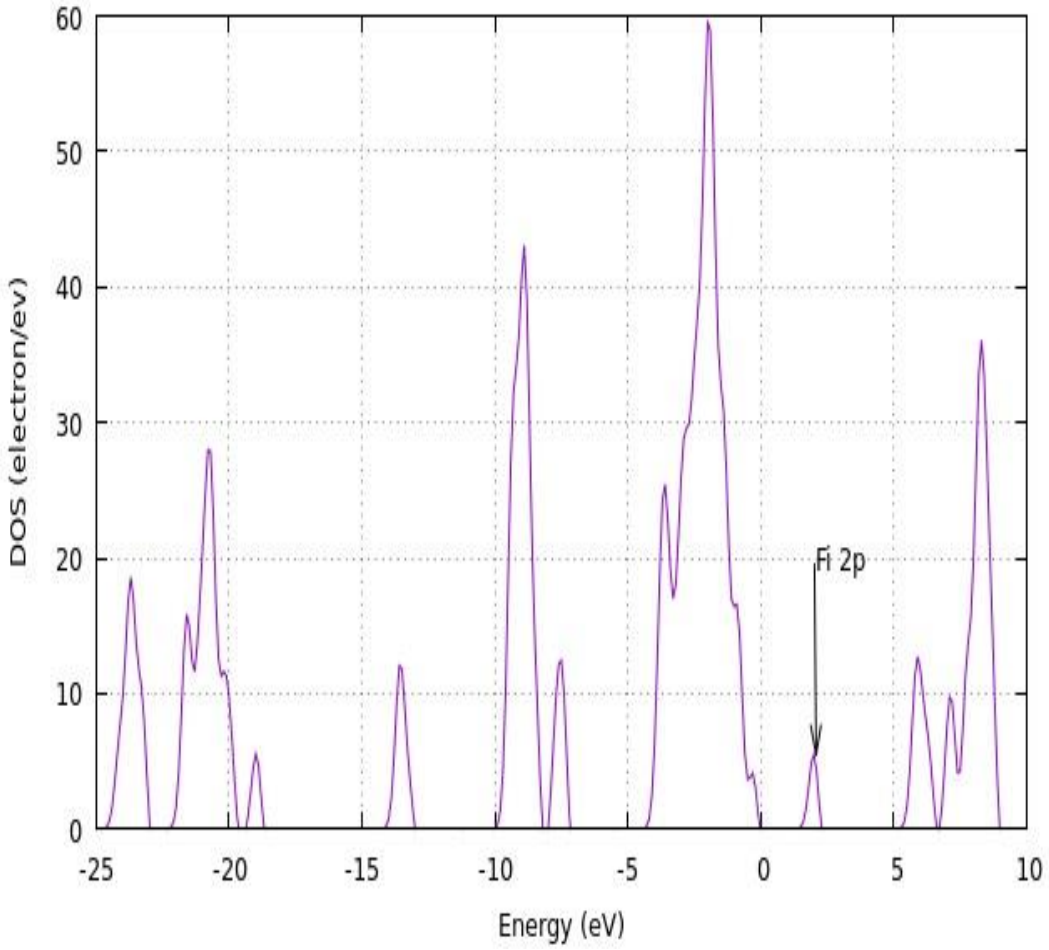

Figure 4. 10: Density of states of BaF_2: La

It is also noted that in the considered energy range, the valence band of this material is formed by F-p state, while the conduction band is dominated by Ba-p and La-p states. The F_i 2p states appear in the forbidden energy region of the host, at the maximum of valence band for BaF_2:La.

Values of the band gap for BaF_2 and BaF_2:La are shown in Table 4.3. A comparison with values from other studies has been made.

Table 4.3: Band gap values for BaF_2 and BaF_2: La

	BaF_2 (eV)	BaF_2:La (eV)	References
GGA	7.38	4.80	This work
HF	7.50	4.68	(Kuznetsov *et al.*,2003)
EXPT	11.0	8.36	(Catlow,1983)

.

From the results obtained, it is noted that the reduction in the band structure is associated to the substitution defect of La and the charge-compensating impurity F_i. A decrease of the band gap from 7.38eV to 4.8eV and an increase in valance band energy from 1.96eV to 2.54eV relative to its value in BaF_2 which is due to the Coulombic interaction between the [La $^{3+}F_i^-$] dipole and its surrounding. The bands were broadened due to the hybridization of the 5d orbital of La with the conduction band minimum and valance band maximum causing additional energy states to form in the BaF_2 band gap.

4.1.5 Mechanical Properties of LaF_3, BaF_2 and BaF_2: La

The elastic constants of solids are important parameters that can provide useful aspects of the mechanical and dynamic characteristics for instance stability and stiffness of a material. The calculated elastic constants for LaF_3, BaF_2 and BaF_2:La at ground state are displayed in table 4.4 and 4.5 respectively.

Table 4. 4 The elastic constants (GPa) and Debye temperature Θ_D for tysoniteLaF$_3$ at ground state

	C_{11}	C_{12}	C_{13}	C_{14}	C_{33}	C_{44}	Θ_D	References
GGA	170.10	76.26	58.69	-1.66	208.07	33.90	383.74	Present
CASTEP	194.33	90.54	60.2	-1.64	240.27	34.28	399.14	(Zhenlong *et al.*,2014)
EXPT	180	88	59	-	222	34	382	(Laiho *et al.*,1983)

The elastic constants obtained are comparable to experimental values. From the results the tysonite crystal is mechanically stable.

Table 4. 5 The Voight-Reuss and Hill's obtained values of the bulk modulus B (GPa), shear modulus G (GPa), Young's modulus E (GPa), B/G and Poisson's ratio (v) for LaF$_3$

	B	G	B/G	E	A	Σ	References
GGA	89.73	46.87	1.91	119.70	0.72	0.276	This work
CASTEP	116.71	49.03	2.38	129.01	-	0.315	(Zhenlong *et al.*,2014)

The value of A calculated for LaF_3 indicates that the materials are highly anisotropic. The values of Poisson's ratio should be of the below 0.1 for covalent bonding and 0.25 for ionic bonding. From the values obtained, LaF_3 is highly ionic. The ratio between B/G known as Pugh' ratio, where B is bulk modulus which indicates fracture resistance and G the shear modulus gives resistance to plastic deformation. The critical value of Pugh's ratio is 1.75. Any value less than this indicates that the

material is brittle in nature(Wu *et al.,* 2017). Our calculated values are greater than 1.75 for these material, indicating that LaF_3 is ductile in nature.

Table 4. 6Elastic constants (GPa) for $BaF_2$and BaF_2:La at ground state

	C_{11}	C_{12}	C_{44}	References
BaF_2	90.00	38.70	24.50	This work
ABINIT	112.40	64.89	28.76	(Schmalzl,2007)
EXPT	98.10	44.81	25.44	(Ravindra *et al.*,2007
BaF_2:La	78.50	31.80	24.50	This work
EXPT	80.80	40.80	25.44	(Rummutla *et al.,* 2015)

The elastic constants for pure BaF_2 are reduced from C_{11}=90.0, C_{12}=38.7, to C_{11}=78.5, C_{12}=31.8, for BaF_2:La except for C_{44} which remains constant. These results indicate reductions in some constants due to enhanced ion mobility (Rummutla *et al.,* 2015).

4.1.6 Defect formation energy of BaF_2: La

When barium atom is substituted with lanthanum atom, a doping of 4% was achieved. This is done with inclusion of charge-compensating interstitial fluorine. When BaF_2 is doped with La, the nearest –neighbor position (NN) or next nearest neighbor (NNN) of interstitial fluorine is obtained. The respective calculated energies are as represented in Tables 4.7 and 4.8.

Table 4. 7: Calculated values of the for defect energy

	Energy (eV)
E_{perf}	-18823.14
E_{La} (defect)	-19456.12607
E_{Ba}	-1026.936
E_{F2}	-658.112
E_{La}	-975.229

Table 4. 8: Defect formation energy

	E_{NN} (eV)	E_{NNN} (eV)	Ref
QE	-26.48	-27.58	This work
HF	-24.76	-25.28	(Kuznetsov *et al.*,2003)

From the defect formation energy obtained, for nearest neighbor(NN)-26.48eV compared to nearest next neighbor(NNN) -27.58eV. From the tabulated results, the interstitial fluorine in the nearest next neighbor gives a more stable structure than when it is in the nearest neighbor position.

4.1.7 Neutral Charge formation energy of BaF_2: La

This process occurs when one atom of barium is substituted with lanthanum without being accompanied by incorporating of charge-compensating interstitial fluorine, but

a neutral charge is included in the calculations. The results obtained are as represented in table 4.9.

Table 4. 9: Calculated neutral charge formation energy

Supercell	Energy
25 atoms without charge	-26.34eV
24 atoms with charge	-25.89eV

From the results obtained the supercell with the charge-compensating fluorine has higher energy compared to the supercell without the charge compensating fluorine. Therefore the supercell without a charge-compensating is more stable than the one with the charge –compensating fluorine. Because Ba is much smaller than a La atom ,it is easier to transport it with less disruption to the structure of the host material, LaF_3. Therefore, it would require less energy to form Ba defects in LaF_3 because with smaller size Ba forms an interstitial easily in LaF_3.

4.1.8 Optical properties of $BaF_2$and BaF_2: La

Optical properties of BaF_2 and BaF_2: La materials were studied with respect to the complex dielectric function. The optical spectrum for BaF_2 and BaF_2:La are as shown in figure 4.11 and 4.12 respectively.

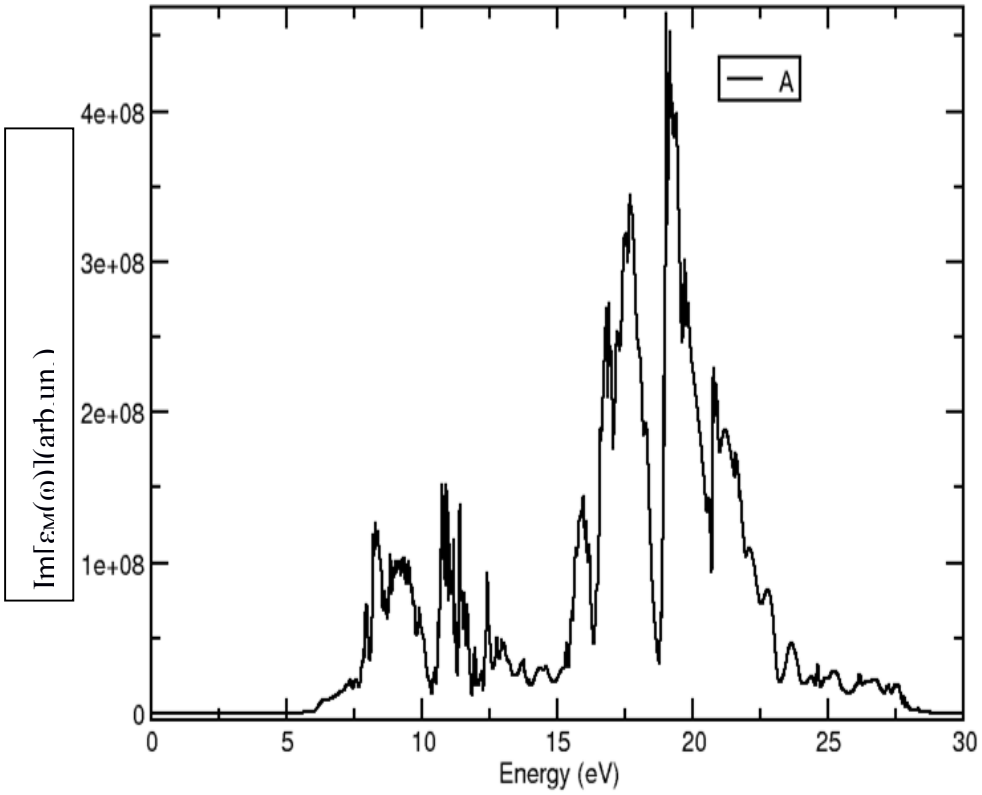

Figure 4. 11: Optical spectrum of BaF_2

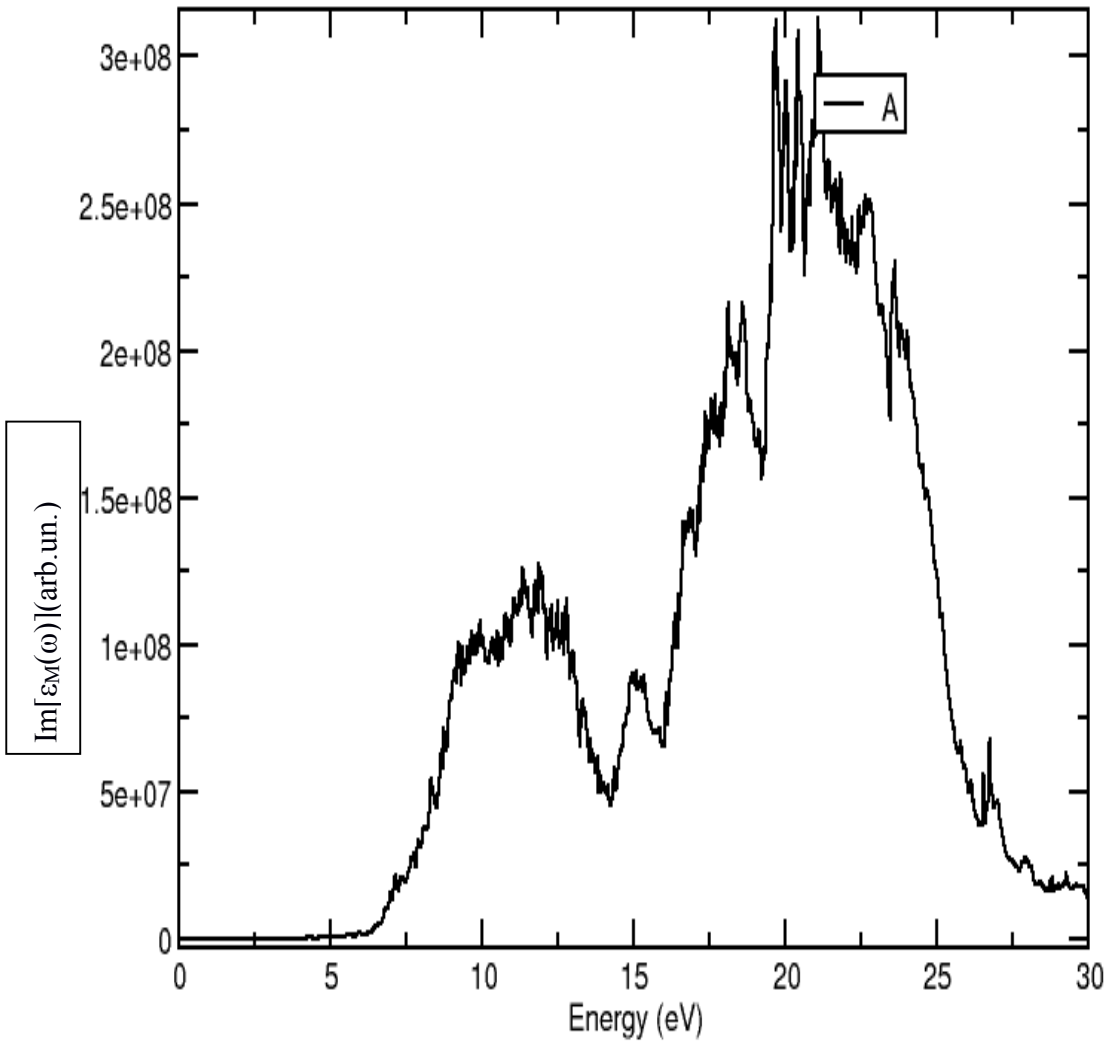

Figure 4. 12: Optical spectrum of BaF_2:La

From the figures, it is noted that the absorption spectrum of BaF_2:La starts at a higher energy compared to that of pure BaF_2.This is attributed to the presence of La atom.

The real and imaginary parts of the refractive indices of BaF_2 and BaF_2:La are presented in figures 4.13 and 4.14 respectively.

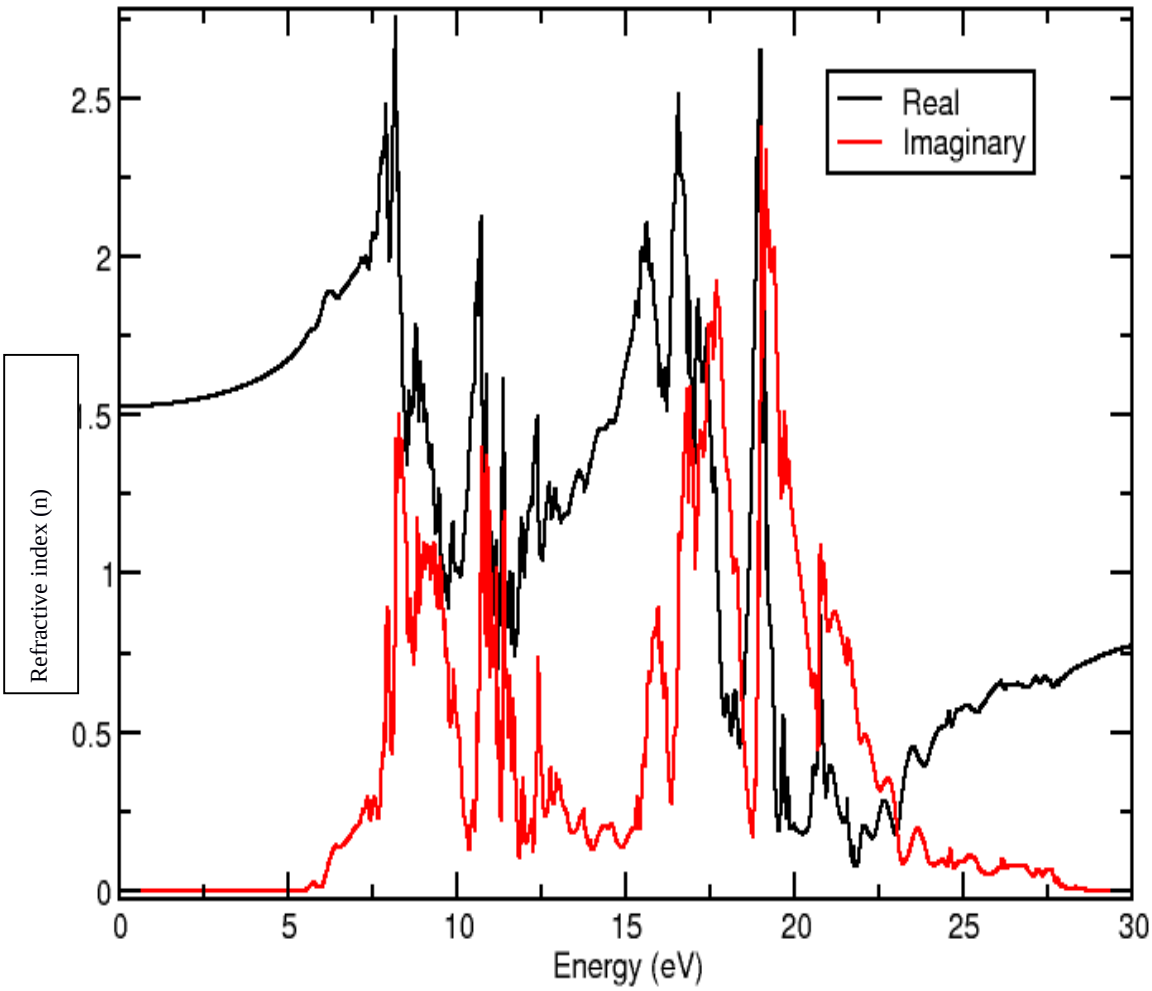

Figure 4. 13: Refractive index of BaF_2

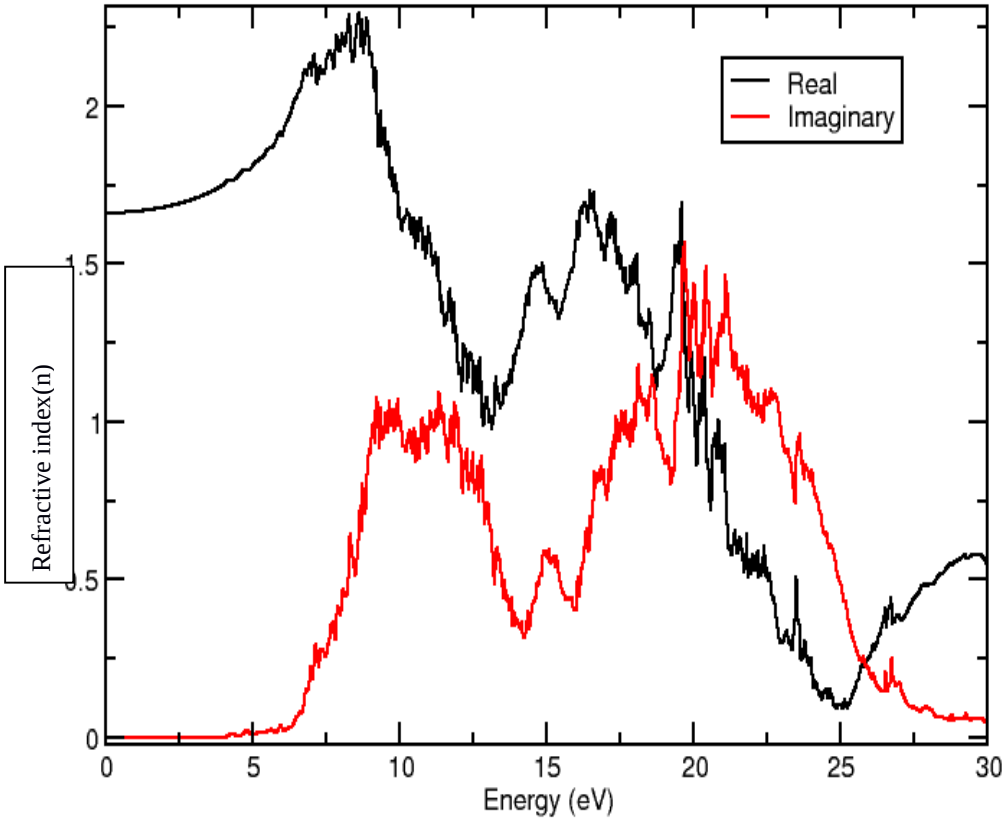

Figure 4. 14 : Refractive index of BaF_2:La

From the figures, the refractive index of BaF_2:La is increased compared to that of pure BaF_2 at 1.58

Table 4. 10*:* Refractive index of BaF_2 and BaF_2:La

	BaF_2	BaF_2:La	References
QE(GGA)	1.52	1.58	This work
GGA+U	1.45	-	(Fooladchang *et al.* ,2013)
EXPT	1.46	1.55	(Weber,2002)

The refractive index of BaF_2 is obtained as 1.52 compared to experimental value of 1.45. The refractive index of BaF_2:La is 1.58 ,this is an increase compared to that of BaF_2. BaF_2:La is therefore useful applications such as lens in lithography.

CHAPTER FIVE

CONCLUSIONS AND RECOMMENDATIONS

5.1 Conclusions

Structural, electronic, mechanical and optical properties were calculated. These were based on the density functional theory which restricts computations to the ground state conditions only. Results of first principles calculations of the electronic, structural, mechanical and optical properties of $LaF_3$and BaF_2:Lapresented in this study were compared with experimental results achieved so far. The calculated results for all the materials in this study are in agreement with experimental findings and they showed consistency with other theoretical predictions

The electronic and structural properties, which were determined from calculations of lattice parameters, bulk moduli, band gap values and density of states were obtained at the ground state. Lattice constants results for LaF_3 are in agreement with experimental results obtained. The Birch Murnaghan third order equation of state gives bulk modulus of 114.44 GPa, which corresponds fairly well with experimental value of 110.4 GPa. The LaF_3 structure is wide band gap of 7.78 eV (direct) while experimental value is 9.1 eV. An indirect band gap of 7.38 eV for$BaF_2$was achieved in this calculation compared to experimental value of 10 eV. The materials studied displayed the properties of insulators from their band structures, and it has been established that semiconductors and insulators tend to have single exchange-correlation potential which is not sufficient enough for such systems where the exchange-correlation potential is likely to be discontinuous across the gap hence the underestimation (Szabo & Ostlund, 1996).

When La was doped in BaF_2, it was noted that there was a reduced band gap. This was due to the introduction of new energy bands in the band structure which was associated with the substitution defect of La and the charge-compensating impurity $F_{i.}$.There was an increase in valance band energy relative to its value in the pure BaF_2 which was due to the Coulombic interaction between the $[La^{3+}\ F_i^-]$ dipole and its surrounding. The elastic constants for pure BaF_2 were obtained as C_{11}=90.0, C_{12}=38.7, C_{14}=24.5 compared to the doped BaF_2: La C_{11} =78.5, C_{12}=31.8, C_{14}=24.5. There is a reduction of C_{11} and C_{12} which is due to the inclusion of the compensating fluorine charge while there is minimal change in C_{44}.These results are an indicator that the changes in the elastic constants were due to enhanced ion mobility (Rummutla, 2015). Doping La in BaF_2 translated to 4% concentration since one La was substituted with one Ba atom. From the defect formation energy obtained, for (NN) -26.48eV compared to (NNN) – 27.58eV. It is observed that the (NNN) is most favorable and stable for dopant La in BaF_2 lattice. Compared to neutral charge formation energy where interstitial fluorine is not included, the formation energy is less than that of included fluorine and thus it is concluded that the neutral charge supercell is more favorable and stable compared to the interstitial supercell.

La affects the electronic properties and hence optical properties of pure BaF_2. As indicated in this study, the absorption spectrum is affected by the presence of the dopant states, the transition from the gap states to conduction band which gives rise to a new absorption spectrum.

5.2 Recommendations

DFT calculations underestimate some electronic properties such as the band gaps. To overcome this challenge of underestimation of band gaps, the GGA+U

pseudopotentials should be used, although they are computationally expensive. However, other approaches may be used to widen the band gaps. Some of these approaches involve the application of the self interacting correction method. This approach involves the removal of the Hatree term that enhances the unphysical self interaction by an orbital-by-orbital correction to the exchange-correlation potential. Calculations that include GW and hybrid functional give better results especially the band gaps. With proper and successful access to high performance computing resources these studies can effectively be carried out at minimal costs.

From the results obtained , BaF_2:La is recommended for use in optoelectronic devices such as solar cells. This is due to the improvement of the optical properties by the dopant. The optical properties results obtained are based on independent particle picture level which may not be comparable to experimental optical spectra directly. La atom is bigger than Ba atom. It is therefore recommended that LaF_3 can be doped with barium atom for future study.

5.3 Suggestions for further studies

1) Further study be done on the optical properties of BaF2:La by inclusion of excitonic effects through the Bethe-Salpeter equations (Sauli, 2011).

2) La atom is bigger compared to Ba atom, there LaF3 can be doped with barium atom and the results compared to this work

REFERENCES

Ambrosch C. and Sofo J.O.(2006). Linear optical properties of solids within the full-potential linearized augmented planewave method. *Comptutational physical communication* 175:1-14

Amolo, G. O. (2018). The Growth of High-Performance Computing in Africa. Computing in Science and Engineering, 20(3):21-24.

Atsushi T. and Isao T.(2015). First principles phonon calculations in Materials science: *Science of Materials*, **108**:1-5.

Belzner A., Schulz H., and Heger G. (1994).The thermal vibrations and the fluorine ionic conductivity in LaF_3.*Kristallographie. Z*eitschrift **2**:209-239

Burke K., (2007).The ABC of DFT Department of Chemistry, University of California, Irvine, CA 92697.

Catlow C. R. A. (1983). Ionicity in solids Comments. *Solid State Physics*. **9**:157-67

Catti M., Dovesi R., Pavese A. and Saunders V.R. (1991). Elastic-constants and electronic-structure of fluorite (CaF2) - An *ab initio* Hartree-Fock study. *Journal of Physics: Condensed Matter* **3:** 4151-4164.

Cottenier S.(2013). Density Functional Theory and the Family of (L)APW-methods: A step-by-step introduction, *Computer Physics Reports*.

Chen D., Wang Y., Yu Y., and Huang P. (2008) Structure and Optical Spectroscopy of Eu-Doped Glass Ceramics Containing GdF3 Nanocrystals. *Journal of Physical Chemistry,* **112**: 18-43.

Clark, S. J., Segall, M. D., Pickard, C. J., Hasnip, P. J., Probert, M. J., Refson, K., & Payne, M. C. (2005). First principles methods using CASTEP. *Zeitschrift für Kristallographie*, *220*(5-6), 567-570. https://doi.org/10.1524/zkri.220.5.567.65075

Crichton W.A., Bouvier P.,Winkler B. and Grzechnik A.(2010).The structural behaviour of LaF_3 at high pressures. *Dalton Trans*.39:4302–4311 DOI: 10.1039/b925817e

Diebold U., (2003).The surface science of titanium dioxide, *Surface Science Report* **48** : 53.

Diniz E.M. and Paschoal C W A.(2007).Structural phase transitions under pressure in rare earth trinorides compounds with tysonite structures. *Solid state communication* **136** : 538-642

Dubinin A., Winkler B., Knorr K. and Milman V., (2004). Lattice dynamics and elastic properties of PbF and BaF from quantum mechanical calculations. *The European Physical Journal B-Condensed Matter and Complex Systems*,**39**(1):27–33

Dyuzheva T.I., Lityagina L.M., Demishev B. and Dendeliani D.A.,(2003). Phase transition and compressibility of LaF3 under pressures up to 40GPa. *Inorganic Matter* **80***:39-59*

Elicah Nafula Wabululu, Nyawere P.W.O.and Daniel Barasa Bem (2018). First-Principles Calculation of Structural, Electronic and Elastic Properties of tysonite Lanthanum Fluoride (LaF_3) *Quest Journal of Research in Environmental and Earth Science*,**104**(1):36-40

Fooladchang F., Majidiyan Sarmazdeh M.,. Benam M.R., and Arabshahi H.(2013)First principles calculations of structural, electronic and optical properties of BaF_2 scintillator crystal at ambient conditions *Physica B,* **427**: 47-52

Gabor Csanyi T.A., Payne M. C. and De Vita A. (2004). Learn on the Fly. A Hybrid Classical and Quantum-Mechanical Molecular Dynamics Simulation. *Physical Review Letters*, **93**:6-8

Gajdoš M., Hummer K. G., Kresse J. and Furthmüller F. (2006). Linear optical properties in the projector-augmented wave methodology. *Physical Review. B* **73** :(045)1-12.

Garcia Sole J., Bausa L.E. and Jaque D. (2005). An Introduction to the Optical Spectroscopy of Inorganic Solids, *Wiley & Sons,* West Sussex, England.

Giannozzi P., Baroni S.,Gironcoli de S. and Dal Corso A. (2001). Phonons and related crystal properties from density-functional perturbation theory. *Reviews of Modern Physics*, **73**(2):515–540

Granqvist G.C. and Hulta ̈ker A.(2002). Transparent and conducting ITO films: new developments and applications, *Thin Solid Films* **411** :1-3.

Harrison W. A.,(1999). Elementary electronic structure, *World Scientific*.

Hill R., (1952). The elastic behaviour of a crystalline aggregate. *Proceeding of Physics Societ. Section* A **65**: 349-354. https://doi.org/10.1088/0370-1298/65/5/307

Hohenberg P. and Kohn W.(1964).Inhomogeneous electron gas. *Physical Review*,**136**:864-871

Huang Y., Chen H., Dong W., Pang F., Wen J., Chen Z., Wang T.,(2016) Fabrication of europium-doped silica optical fiber with high verdet constant, Optical Express **24** (16) :18709-18717.

Itoh M. and Itoh H. (1992).The surface science of titanium dioxide, *Physical. Review*. B **46** (15):509-511

Joubert M.F., Guyot, Y., Jacquier B., Chaminade J.P., and Garcia A.(2005) "Fluoride Crystals and high lying excited states of rare earth ions," *Journal of Fluorine Chemistry* 107- 235.

Kang I. Y., Yoon-Suk Kim, Yong-Chae Chung, Deok-Soo Kim H. Kim and Jay J. (2002).*Kim* **3** :171–173

Keen D.A. , Hull S., Barnes A.C., Berastegui P., Crichton W.A., MaddenP.A. , Tucker M.G., and Wilson M. (2000). Nature of the superionic transition in Ag + and Cu + halides, *Physical Review. B,* **68** (014):1-17.

Kohn W. and Sham L.J., (1965) Self-consistent equations including exchange and correlation effects *Physics Review* **140** (4A):A1133 -A1138

Knauth P. and Tuller H.(2002) Solid-State Ionics: Roots, Status, and Future Prospects. *Journal of the American Ceramic Society* **85**: (7)1654–1680

Kuneš J., Novák P., Schmid R., Blaha P., and Schwarz K., (2001). Electronic structure of fcc The Spin-orbit calculation with 6p1/2local orbital extension. *Physical Review B - Condensed Matter Materials. 64:* 1531021–1531023. https://doi.org/ 10.1103

Kuznetsov A., Sobolev A.B., Varaksin A.N., Andriessen J. and Van Eijk C.W.E.,(2003) First -principles Calculations of the Electronic and Spatial Structures of the Ba1-x $LaxF_{2+x}$ system within the supercell Model, *Physics of solid state* 45(5):15-23

Labeguerie J . , GredinP., M. Mortier, Patriarche G., and A. de Kozak, (2006) "Syntheses of Fluoride Nanoparticles in Non-Aqueous Nanoreactors. Luminescence Study of Eu^{3+}:CaF_2," *Zeitschrift fur anorganische and allgemeine Chemie,* **632**:15-38.

Laiho R., and Lakisto M., (1983).Investigation of refractive indices of LaF_3, CeF_3,PrF_3 NdF_3.*Phil.Magazine B.48*.

Lian H., Liu J., Ye Z., and Shi C.,(2004). Synthesis and photoluminescence properties of erbium-doped BaF2 nanoparticles. *Chemical Physics Letters*, **386**:291-302.

Limpijumnong S. and Van de Walle C.G.(2004). Diffusivity of native defects in gas. *Physical Review B***, 69**(3):035207-035301.

Lundstrom M.(2002). Fundamentals of Carrier Transport. *Measurement Science Technology* https://doi.org/ 10.1088/0957-0233/13/2/703

Makau N. W.,(2006). Foreign Atoms on the Three Low Index Diamond Surfaces. PhD thesis, University of the Witwatersrand, Johannesburg.

Manjula, M., Sundareswari M., Viswanathan, E.,(2016). Enhancement of ductility in cubic Rh3AxTi1x(A = V, Nb, Ta)(x = 0, 0.125, 0.25, 0.75, 0.875, 1)aerospace materials–First principles DFT study. *Mater. Chem. Phys. 181*, 90–98. https://doi.org/10.1016/j.matchemphys.2016.06.037

Masoud Majidiyan, Javad Baedi, M R Benam, (2010) First-principles study of the effect of La substitution on the electronic and optical properties of Pb(ZrxTi1−x)O3 crystal. *Physical Sciences*. 81: 035701-035706.

Mattausch A.(2005). *Ab initio*-Theory of Point Defects and Defect Complexes in SiC.

Mattsson M.T.,(2011). High-performance computing for materials design to advance energy science. *MRS Bulleting* **36**: 169-174.

Modak P., Verma A.K., Ghosh S. and Das G.P.(2009). Pressure induced phase transition in tysonite LaF_3.*Physical Chemistry Solids* **70** :922-923

Monkhorst H. and Pack J.,(1976) .Special points for Brillouin-zone integrations. *Phys. Rev*. *B* **13** (12): 5188–5192.

Morris E., Groy T., and Leinenweber K. (2001) Crystal structure and bonding in the high-pressure form of fluorite (CaF2). *Journal of Physics and Chemistry of Solids*, **62**(6):1117-1122

Nepomnyashchikh A.I., Radzhabov E.A., Egranov V. and Ivashechkin V.F. (2001).Defect formation and VUV luminescence in BaF2. *Radiation. Measurement. 33:759-765*

Niu L. and Mueller T. (2016).Bayesian cluster expansion with lattice parameter dependence for studying surface alloys. *Bulletin of American Physical Society*

Nyawere P.W.O., Makau N.W. and Amolo G.O.(2014).*Ab initio* calculations of electronic and mechanical properties of orthorhombic phase of BaF_2. *Physica B* **434**:34-36

Parr R.G. and Yang W.,(1995). Density-functional theory of the electronic structure of molecules. *Annual Review of Physical Chemistry*, **46**:701-728

Payne M.C., Teter M.P., Allen D.C., Arias T.A., and Joannopoulous J.D. (1992). Iterative minimization techniques for ab initio total-energy calculations: molecular dynamics and conjugate gradients. *Reviews of Modern Physics,* **64**(4): 1045-1097.

Paier J., Marsman M., Hummer K., Kresse G., GerberI. C. and. ´Angya´n J. G, J. (2006) *Chemical Physics*.**124** :154709-154720.

Petit, V., Camy P., Doualana J.L., and Moncorge R.,(2006) Cw and tunable laser operation of Yb^{3+}in Nd:Yb:CaF2. *Applied Physics Letters*, **88**:(051)1-11.

Perdew J. P., Burke K., Ernzerhof M., (1996) .Generalized gradient Approximation made Simple *Phyical Review Letters.* **80** (4) 891–891

Rammutla K.E., Comins J.D Ngoepe ., P.E. and ChadwickA.V. (2015).Structural and optical characterization of double -doped TiO_2 nanoparticles. *Radiation Effects in Defects Solids* **15**:77-83

Ravindran P., Vajeeston P., Vidya R., Kjekshus A., and H. Fjellva H.(2001).Detailed electronic structure studies on superconducting MgB_2 and related compounds. *Physical Review B,* **64**(22):224-509

Rappoport, F.F.(2005). Density functional methods for excited states: equilibrium structure and electronic spectra. *Theoretical and Computational Chemistry,* **16**:93-128.

Reuss A.,(1929). Berechnung der Fließgrenze vonMischkristallen auf Grund der Plastizitätsbedingung fürEinkristalle . ZAMM - *Journal of Applied Mathematics for Mechanics. /Zeitschrift für Angew. Math. und Mech*. 9, 49-58. https://doi.org/ 10.1002/zamm.19290090104

Safronikhin A. V., Ehrlich G. V., and LisichkinG. V.(2011).Synthesis of Lanthanum Fluoride Nanocrystals. *Russian Journal of General Chemistry* **81**: (02) 277–281

Sahoo B.D. , JoshiK. D. and GuptaS.C.(2017).Ab intio study on pressure induced structural sequences in LaF3 up to 2 Mbar. *AIP Conference Proceedings* 1665 030028. doi:10.1063/1.4917603

Sata N., Eberman K., Eberl K., and Maier J., ,(2000). Mesoscopic fast ion conduction in nanometre-scale planar heterostructures. *Nature,* **408**(6815): 946–949

Sauli, V. Solving the BSE with an Integral Representation in Minkowski Space. *Few-Body Syst* **49,** 223–231 (2011). https://doi.org/10.1007/s00601-010-0118-4

Scandolo S., Gannozzi P., Cavazzoni C., Gironcoli S. de, Pasquarello A. and Baroni S., Z. (2005).First principles codes for computational crystallography in Quantum espresso package. *kristallographie,* **220**:574-579

Schmalzl K. (2007).Volume and pressure dependence of ground-state and lattice-dynamical properties of BaF_2 from density-functional methods *Physical Review B* **75** (1):143-156.

SinitsynV.V., Lips O., Privalov A.F., Fujara F., Murin I.V.,(2003). Transport properties of LaF3 fast ionic conductor studied by field gradient NMR and impedence spectroscopy. *Physical Chemistry of Solids* **64**:1201-1207

Sin'ko G. V. and Smirnow N.A.(2002).*Ab intio* calculations of elastic constants and thermodynamic properties of bcc,fcc and hcp Al crystals under pressure. *Physical Condensed Matter***168**:23-48

Shi H., Eglitis R., and Borste lG.,(2006). *Ab* initio calculations of the BaF_2 bulk and surface f centres, *Physical Condensed Matter* **18** (35): 67-83.

Sholl J.A.S., and David S. (2009). Density Functional Theory: A Practical Introduction. *Wiley*. 238.

Shrader, D., Szlufarska I., and Morgan D.(2012). Cs diffusion in cubic silicon carbide. *Journal of Nuclear Materials* **421**(1–3): 89-96.

Sobolev A.B., Kuznetsov, A.Yu., Andriessen, J., van Eijk, C.W.E. (2002). Hartree-Fock calculation of BaF_2:La systems. *Nuclear Instrumentation Methods* A **486**:385-389

Smallwood J.C., William R.E.L., Glover J., Benjamin J. and Schwartz A. (2006). A computationally efficient exact pseudopotential method. I. Analytic reformulation 67 of the Phillips-Kleiman theory. *The Journal of Chemical Physics* 12: 074102-074111.

Stefano Curtarolo, Gus LW Hart, Marco Buongiorno Nardelli, Natalio Mingo, Stefano Sanvito, and Ohad Levy (2013). The high-throughput highway to computational materials design . *Nature materials*, **12**(3):191-201

Taki Y. and Muramatsu K.,(2002) .Hetero-epitaxial growth and optical properties of LaF_3 on CaF_2,*Thin Solid Films* **420** (421): 30-33

Chung D. H,. and Buessem W.R (1967).The Voigt-Reuss-Hill Approximation and Elastic Moduli of polycrystalline Mgo,CaF2,Zns,ZnSe and CdTe. *Journal of physics* **36**:25-35

Wang, F. Fan, X. Pi, D. and Wang, M.(2005). Synthesis and luminescence behavior of Eu3+-doped CaF2 nano-particles. *Solid State Communications*, **133**: 775-778

Wang S.Q. and Ye H.Q.(2003) *Ab initio* elastic constants of C, Si, Ge. *Journal of Physics: Condensed Matter*, **15**:5307–5314

Wang Z.L., Quan Z.W., Jia, P.Y., Lin C.K., Luo, Y., Chen Y., Fang, J., Zhou W., O'Connor C.J. and Lin J. (2006). A Facile Synthesis and Photoluminescent Properties of Redispersible CeF_3, CeF3:Tb^{3+} and CeF_3:$Tb^{3+/}LaF_3$ (Core/Shell) Nanoparticles, *Chemistry of Materials*, **18** :20-30 .

Winkler B., Knorr K., MilmanV., (2003). Prediction of the structure of LaF_3 at high pressures. *Journal of Compounds* **349**: 1-11

Wu S.C., Naghavi, S.S., Fecher, G.H. and Felser, C.,(2017). A critical study of the elastic properties and stability of Heusler compounds: Phase change and tetragonal $X_{2}YZ$ compounds 775–805. *https://doi.org/ 10.4236/jmp.2018.94050*

Zhenlong L.V, Cai Cheng Yan Cheng, Chen Xiangrong, Ji Gaungfu (2014).Elastic, thermodynamic and electronic properties of LaF_3 under pressure from first principles. *Computational Material Science* **89**: 57-60

APPENDICES

APPENDIX I: Input file for pwscf code tysonite LaF_3 structure

```
&CONTROL
calculation='scf'
restart_mode='from_scratch',
pseudo_dir = "./",
outdir='./tmp',
prefix='LaF3'
/
&SYSTEM
ibrav = 4,
celldm(1) =13.69,
celldm(2)=1.02,
nat= 24, ntyp= 2,
ecutwfc = 60,ecutrho = 720.0,
occupations='smearing',
 smearing='marzari-vanderbilt', degauss=0.0
 /
&ELECTRONS
mixing_beta = 0.7
/
 ATOMIC_SPECIES
La 138.9054La.pbe-nsp-van.UPF
F  19.998403   F.pbe-nsp-van.UPF
ATOMIC_POSITIONS (crystal)
La      0.95174600000000   0.63376300000000   0.75000000000000
La      0.45174600000000   0.86623700000000   0.25000000000000
La      0.54825400000000   0.13376300000000   0.75000000000000
La      0.04825400000000   0.36623700000000   0.25000000000000
La      0.6608985110000    0.00000000000000   0.25000000000000
La       0.3391014890000     0.3391014890000   0.75000000000000
F       0.36211400000000   0.16294300000000   0.43648800000000
F       0.86211400000000   0.33705700000000   0.56351200000000
F       0.13788600000000   0.66294300000000   0.06351200000000
F       0.63788600000000   0.83705700000000   0.93648800000000
F       0.60951100000000   0.52897100000000   0.25000000000000
F       0.10951100000000   0.97102900000000   0.75000000000000
F       0.89048900000000   0.02897100000000   0.25000000000000
F       0.39048900000000   0.47102900000000   0.75000000000000
F       0.36211400000000   0.16294300000000   0.06351200000000
F       0.86211400000000   0.33705700000000   0.93648800000000
F       0.13788600000000   0.66294300000000   0.43648800000000
F       0.63788600000000   0.83705700000000   0.56351200000000
F      0.94637209600000    0.31331301620000  0.08175839200000
F       0.3667580660000   0.053627904000000  0.08175839200000
F       0.3667580660000   0.053627904000000  0.91817583920000
K_POINTS automatic
 9 7 5  1 1 1
```

APPENDIX II: Input file for pwscf code Supercell BaF_2 structure

```
&CONTROL
calculation='scf'
restart_mode='from_scratch',
pseudo_dir = "./",
outdir='./tmp',
prefix='LaF3'
/
&SYSTEM
ibrav = 2,
celldm(1) =16.69,
nat= 24, ntyp= 2,
ecutwfc = 60,ecutrho = 720.0,
 !occupations='smearing', smearing='marzari-vanderbilt', degauss=0.0
 /
&ELECTRONS
mixing_beta = 0.7
/
 ATOMIC_SPECIES
Ba 137.34    Ba.pbe-nsp-van.UPF
F  19.998403   F.pbe-nsp-van.UPF

ATOMIC_POSITIONS (crystal)
La      0.95174600000000   0.63376300000000   0.75000000000000
La      0.45174600000000   0.86623700000000   0.25000000000000
La      0.54825400000000   0.13376300000000   0.75000000000000
La      0.04825400000000   0.36623700000000   0.25000000000000
La      0.6608985110000    0.00000000000000   0.25000000000000
La       0.3391014890000     0.3391014890000   0.75000000000000
F       0.36211400000000   0.16294300000000   0.43648800000000
F       0.86211400000000   0.33705700000000   0.56351200000000
F       0.13788600000000   0.66294300000000   0.06351200000000
F       0.63788600000000   0.83705700000000   0.93648800000000
F       0.60951100000000   0.52897100000000   0.25000000000000
F       0.10951100000000   0.97102900000000   0.75000000000000
F       0.89048900000000   0.02897100000000   0.25000000000000
F       0.39048900000000   0.47102900000000   0.75000000000000
F       0.36211400000000   0.16294300000000   0.06351200000000
F       0.86211400000000   0.33705700000000   0.93648800000000
F       0.13788600000000   0.66294300000000   0.43648800000000
F       0.63788600000000   0.83705700000000   0.56351200000000
F      0.94637209600000    0.31331301620000   0.08175839200000

 K_POINTS automatic
 9 9  9 1 1 1
```

APPENDIX III: Input file for pwscf code Supercell BaF_2:La

```
&CONTROL
Calculation='scf'
restart_mode='from_scratch',
pseudo_dir = "./",
outdir='./tmp',
prefix='LaF3'
/
&SYSTEM
ibrav = 2,
celldm(1) =16.69,
nat= 25, ntyp= 3,
ecutwfc = 60,ecutrho = 720.0,
 !occupations='smearing',
 smearing='marzari-vanderbilt',
 degauss=0.0
 /
&ELECTRONS
mixing_beta = 0.7
/
 ATOMIC_SPECIES
Ba 138.9054   Ba.pbe-nsp-van.UPF
La 138.9054    La.pbe-nsp-van.UPF
F  19.998403   F.pbe-nsp-van.UPF
ATOMIC_POSITIONS (crystal)
Ba      0.95174600000000   0.63376300000000   0.75000000000000
Ba      0.45174600000000   0.86623700000000   0.25000000000000
Ba      0.54825400000000   0.13376300000000   0.75000000000000
La      0.04825400000000   0.36623700000000   0.25000000000000
Ba      0.6608985110000    0.00000000000000   0.25000000000000
Ba       0.3391014890000     0.3391014890000   0.75000000000000
F       0.36211400000000   0.16294300000000   0.43648800000000
F       0.86211400000000   0.33705700000000   0.56351200000000
F       0.13788600000000   0.66294300000000   0.06351200000000
F       0.63788600000000   0.83705700000000   0.93648800000000
F       0.60951100000000   0.52897100000000   0.25000000000000
F       0.10951100000000   0.97102900000000   0.75000000000000
F       0.89048900000000   0.02897100000000   0.25000000000000
F       0.39048900000000   0.47102900000000   0.75000000000000
F       0.36211400000000   0.16294300000000   0.06351200000000
F       0.86211400000000   0.33705700000000   0.93648800000000
F       0.13788600000000   0.66294300000000   0.43648800000000
F       0.63788600000000   0.83705700000000   0.56351200000000
F      0.94637209600000    0.3133130162000    0.08175839200000
F       0.3667580660000   0.05362790400000    0.08175839200000
K_POINTS automatic
 9 9  9 1 1 1
```

APPENDIX IV: Input file for pwscf code Supercell BaF_2:La with neutral charge

```
&CONTROL
Calculation='scf'
restart_mode='from_scratch',
pseudo_dir = "./",
outdir='./tmp',
prefix='LaF3'
/
&SYSTEM
ibrav = 2,
celldm(1) =16.69,
nat= 24, ntyp= 3,
ecutwfc = 60,ecutrho = 720.0,
occupations='smearing',
charge tot= +1
 smearing='marzari-vanderbilt',
 degauss=0.0
 /
&ELECTRONS
mixing_beta = 0.7
/
 ATOMIC_SPECIES
Ba 138.9054   Ba.pbe-nsp-van.UPF
La 138.9054    La.pbe-nsp-van.UPF
F  19.998403   F.pbe-nsp-van.UPF
ATOMIC_POSITIONS (crystal)
Ba      0.95174600000000   0.63376300000000   0.75000000000000
Ba       0.45174600000000   0.86623700000000   0.25000000000000
Ba       0.54825400000000   0.13376300000000   0.75000000000000
La       0.04825400000000   0.36623700000000   0.25000000000000
Ba       0.6608985110000     0.00000000000000   0.25000000000000
Ba        0.3391014890000      0.3391014890000   0.75000000000000
F        0.36211400000000   0.16294300000000   0.43648800000000
F        0.86211400000000   0.33705700000000   0.56351200000000
F        0.13788600000000   0.66294300000000   0.06351200000000
F        0.63788600000000   0.83705700000000   0.93648800000000
F        0.60951100000000   0.52897100000000   0.25000000000000
F        0.10951100000000   0.97102900000000   0.75000000000000
F        0.89048900000000   0.02897100000000   0.25000000000000
F        0.39048900000000   0.47102900000000   0.75000000000000
F        0.36211400000000   0.16294300000000   0.06351200000000
F        0.86211400000000   0.33705700000000   0.93648800000000
F        0.13788600000000   0.66294300000000   0.43648800000000
F        0.63788600000000   0.83705700000000   0.56351200000000
F       0.94637209600000     0.3133130162000    0.08175839200000
F        0.3667580660000    0.05362790400000    0.08175839200000
K_POINTS automatic
 9 9   9 1 1 1
```

APPENDIX V: Publications

1) Elicah Nafula Wabululu, P.W.O Nyawere, Daniel Barasa Bem Scientific Research Through Simulation in Africa: Role of HPC in Computational Material Studies. International Journal of Materials Science and Applications.Vol.6,No.4,2017,pp.190192.doi:10.11648/j.ijmsa.20170604.14

2) Elicah Nafula Wabululu, P.W.O Nyawere Daniel Barasa Bem First-Principles Calculation of Structural, Electronic and Elastic Properties of tysonite Lanthanum Fluoride (LaF_3) Quest Journal of Research in Environmental and Earth Science,vol.04 No.1,2018,pp 36-40